The Astrophysical Journal, 919:16 (22pp), 2021 September 20 https://doi.org/10.3847/1538-4357/ac0e95

Measurements of the Hubble Constant: Tensions in Perspective*

Wendy L. Freedman
Department of Astronomy & Astrophysics & Kavli Institute for Cosmological Physics, University of Chicago, 5640 South Ellis Avenue, Chicago, IL 60637, USA
wfreedman@uchicago.edu
Received 2021 May 17; revised 2021 June 20; accepted 2021 June 23; published 2021 September 17

Abstract

Measurement of the distances to nearby galaxies has improved rapidly in recent decades. The ever-present challenge is to reduce systematic effects, especially as greater distances are probed and the uncertainties become larger. In this paper, we combine several recent calibrations of the tip of the red giant branch (TRGB) method. These calibrations are internally self-consistent at the 1% level. New Gaia Early Data Release 3 data provide an additional consistency check at a (lower) 5% level of accuracy, a result of the well-documented Gaia angular covariance bias. The updated TRGB calibration applied to a sample of Type Ia supernovae from the Carnegie Supernova Project results in a value of the Hubble constant of $H_0 = 69.8 \pm 0.6$ (stat) $\pm$ 1.6 (sys) km s^{-1} Mpc^{-1}. No statistically significant difference is found between the value of H_0 based on the TRGB and that determined from the cosmic microwave background. The TRGB results are also consistent to within 2σ with the SHoES and Spitzer plus Hubble Space Telescope (HST) Key Project Cepheid calibrations. The TRGB results alone do not demand additional new physics beyond the standard (ΛCDM) cosmological model. They have the advantage of simplicity of the underlying physics (the core He flash) and small systematic uncertainties (from extinction, metallicity, and crowding). Finally, the strengths and weaknesses of both the TRGB and Cepheids are reviewed, and prospects for addressing the current discrepancy with future Gaia, HST, and James Webb Space Telescope observations are discussed. Resolving this discrepancy is essential for ascertaining if the claimed tension in H_0 between the locally measured and CMB-inferred values is physically motivated.

Unified Astronomy Thesaurus concepts: Cosmology (343); Hubble constant (758); Cepheid variable stars (218); Red giant stars (1372); Stellar distance (1595); Observational cosmology (1146)

1. Introduction

Over the last decade, the unprecedented increase in accuracy obtained by a broad range of independent cosmological experiments and observations has provided striking and compelling support for our current standard Λ cold dark matter (ΛCDM) model. This concordance cosmology has been remarkably successful in explaining an even wider range of observations, from the exquisite precision in recent measurements of fluctuations in the temperature and polarization of the cosmic microwave background (CMB) radiation (Aiola et al. 2020; Planck Collaboration et al. 2020) to observations of large-scale structure and matter fluctuations in the universe (e.g., baryon acoustic oscillations, BAO; Macaulay et al. 2019).

However, as the accuracy of both the observations and the tests of ΛCDM has improved, a number of discrepancies have been noted. The most apparently significant of these is the claim of a tension between competing values of the Hubble constant (H_0), where the discrepancy is currently estimated to be at the 5σ–6σ level (Di Valentino et al. 2021; Riess et al. 2021) between the local values of H_0 and those derived from models of the CMB.[1] This claimed tension suggests that the universe at present is expanding about 8% faster than predicted assuming the ΛCDM model, which, if confirmed, could provide evidence for cracks in the standard model, offering the exciting opportunity for discovering new physics. Confirming the reality of the H_0 tension could have significant consequences for both fundamental physics and modern cosmology.[2] The implications of an accurate value of H_0 are of interest, however, independently of how the tension is ultimately resolved; providing independent confirmation of the standard cosmological model would also be a critical result.

As apparent fissures in the standard model have been emerging, there are also indications that there may be cracks that need attention in the local distance scale as well. For example, the tip of the red giant branch (TRGB) method and the Cepheid distance scale result in differing values of $H_0 = 69.6 \pm 1.9$ km s^{-1} Mpc^{-1} (Freedman et al. (2019, 2020, hereafter F19, F20) for the TRGB and 73.2 ± 1.3 (Riess et al. 2021, hereafter R21) for the Cepheids. This divergence raises the question of whether the purported tension is being driven by yet-to-be-revealed systematic errors in the local Cepheid data rather than in the cosmological models.

A number of measurements of H_0 calibrated locally (referred to as late-time estimates) exhibit reasonable agreement to

* Based on observations made with the NASA/ESA Hubble Space Telescope, obtained at the Space Telescope Science Institute, which is operated by the Association of Universities for Research in Astronomy, Inc., under NASA contract NAS 5-26555. These observations are associated with program Nos. 13472, 13691, 9477, and 10399.

[1] As noted by Feeney et al. (2018), the true tension between the Planck and SHoES results depends on accurate knowledge of the tails of the likelihoods of the two distributions, rather than assuming them to be Gaussian. The significance of the current tension also depends on the assumption that all sources of uncertainty have been recognized and accounted for.

[2] For a different perspective on the H_0 tension, see the recent review by Linder (2021).

within their quoted uncertainties, generally falling in the range of 70–76 $\mathrm{km\,s^{-1}\,Mpc^{-1}}$ (Freedman et al. 2012, 2019, 2020; Riess et al. 2016, 2019; Reid et al. 2019; Huang et al. 2020; Kourkchi et al. 2020; Pesce et al. 2020; Blakeslee et al. 2021; Khetan et al. 2021). In contrast, (early-time) estimates of H_0 based on measurements of fluctuations in the temperature and polarization of the CMB from Planck and ACT+WMAP (Aiola et al. 2020; Planck Collaboration et al. 2020) consistently yield lower values of $H_0 = 67.4 \pm 0.5$ and 67.6 ± 1.1 $\mathrm{km\,s^{-1}\,Mpc^{-1}}$, respectively, both adopting the current standard ΛCDM model. Measurements of fluctuations in the matter density or BAOs (e.g., Aubourg et al. 2015; Macaulay et al. 2019) also result in similar (low) values if the absolute scale is set by the sound horizon measurement from the CMB or by Big Bang nucleosynthesis (BBN) constraints, also based on sound horizon physics.

High values of H_0 were initially obtained from time-delay measurements of strong gravitational lensing (Suyu et al. 2017; Wong et al. 2020), with $H_0 = 73^{+1.7}_{-1.8}$ $\mathrm{km\,s^{-1}\,Mpc^{-1}}$, apparently consistent with the Cepheid measurements. However, recent detailed consideration of the assumptions in the modeling of the lens mass distribution (Birrer & Treu 2021; Birrer et al. 2020) leads to a much lower value of the Hubble constant, as well as a significantly larger value of the uncertainty, $H_0 = 67.4^{+4.1}_{-3.2}$ $\mathrm{km\,s^{-1}\,Mpc^{-1}}$, currently consistent with the CMB and TRGB measurements.

The debate over the value of the Hubble constant is clearly not yet over. And with the high precision of current CMB measurements, the requirement for greater accuracy in the local value of H_0 has grown substantially. Given the importance of this question for fundamental physics and cosmology, and given the history of H_0 and the century-long effort to address a multiplicity of systematic effects, it is essential that rigorous tests be undertaken to investigate the possibility that remaining (potentially unknown) systematic errors are responsible for driving the controversy.

The TRGB method has emerged as one of the most precise and accurate means of measuring distances in the local universe. The TRGB is an excellent standard candle, an unambiguous signpost of the core helium flash luminosity at the end phase of red giant branch (RGB) evolution for low-mass stars (e.g., Lee et al. 1993; Salaris et al. 2002; Rizzi et al. 2007; Madore et al. 2009; Freedman et al. 2019; Jang et al. 2021). Empirically, observed color–magnitude diagrams (CMDs) of the halos of nearby galaxies reveal a sharp discontinuity at a well-defined luminosity.

In F19, we presented a determination of H_0 based on TRGB distances to 15 galaxies that were hosts to 18 Type Ia supernovae (SNe Ia). The *I*-band TRGB distances were measured using Hubble Space Telescope (HST) Advanced Camera for Surveys (ACS) data targeting the halo regions of nearby galaxies and then applied to a sample of 99 significantly more distant SNe Ia (out to $z = 0.08$) that were observed as part of the Carnegie Supernova Project (CSP) and published in Krisciunas et al. (2017). This TRGB calibration was updated slightly in F20, yielding a value of $H_0 = 69.6 \pm 0.8$ (stat) $\pm$ 1.7 (sys) $\mathrm{km\,s^{-1}\,Mpc^{-1}}$. To date, the TRGB is the only method with comparable numbers of galaxies in its calibration relative to Cepheids; the H_0 calibration of Riess et al. (2016, 2019, hereafter R16, R19) is based on the Cepheid distances to 19 galaxies. Ten of the galaxies in the F19 and F20 TRGB sample also have independent Cepheid distances, an order-of-magnitude greater number than for Miras (Huang et al. 2020) or the maser technique (Pesce et al. 2020), which are both cases where only a single galaxy is available for comparison with Cepheids.

The immediate goal of this paper is to update the F20 TRGB calibration of H_0, which was based solely on a geometric distance to the Large Magellanic Cloud (LMC). In the interim, a number of detailed new studies of the giant branch population in our own and several nearby galaxies can now provide new and independent calibrations of the TRGB. Five independent calibrations are examined in this paper, as follows.

1. Observations of the TRGB in the outer halo of the maser galaxy, NGC 4258 (Jang et al. 2021).
2. Observations of TRGB stars in 46 Galactic globular clusters spanning a range of metallicities (Cerny et al. 2020), calibrated via a detached eclipsing binary (DEB) distance to ω Cen.
3. A new geometric distance to the Small Magellanic Cloud (SMC) based on an augmented sample of 15 DEBs (Graczyk et al. 2020), incorporating the updated reddening and extinction maps of Skowron et al. (2021), together with an updated measurement of the TRGB magnitude by Hoyt (2021).
4. A reanalysis of the OGLE-III data for the LMC by Hoyt (2021), incorporating the updated reddening and extinction maps of Skowron et al. (2021).
5. New Magellan imaging data for two Milky Way dwarf spheroidal galaxies, Sculptor (Tran et al. 2021) and Fornax (Oakes et al. 2021), as well as HST/ACS published data for four LMC globular clusters (Olsen et al. 1998) providing an additional check on the calibration of the TRGB zero-point.

A second goal of this paper is to examine and compare recent calibrations of the TRGB and Cepheid distance scales; finally, a third goal is to assess the significance of the tension in H_0 as it currently stands.

The outline of this paper is as follows. In Section 2, we describe the recent calibrations of the TRGB; in Section 3, we discuss the implications of these results in the context of the determination of H_0; and in Section 4, we summarize recent calibrations of the Cepheid Leavitt law. We then compare the H_0 values in Section 5, and finally, in Section 6, we discuss the current status, strengths, and weaknesses in the TRGB and Cepheid distance scales before comparing our results with other methods in Section 7 and summarizing our results in Section 8.

In brief, based on four independent calibrations of the TRGB absolute magnitude, we find $M^{\mathrm{TRGB}}_{\mathrm{F814W}} = -4.049 \pm 0.015$ (stat) $\pm$ 0.035 (sys) mag, leading to a value of $H_0 = 69.8 \pm 0.6$ (stat) $\pm$ 1.6 (sys) $\mathrm{km\,s^{-1}\,Mpc^{-1}}$. Accurate calibration of the extragalactic distance scale remains a challenging endeavor, and <1% measurements of the CMB set a high (and currently not attainable) bar for the local distance scale to match. The discrepancy in local (TRGB versus Cepheid) measurements suggests that there are issues in the local distance scale that need to be understood before we can unambiguously make extraordinary claims like new physics.

Table 1
Absolute *I*-band TRGB Calibrations

$M^I_{\rm TRGB}$[a]	References
-4.0 ± 0.1	Lee et al. (1993)
-4.05[b]	Rizzi et al. (2007)
-4.04[c]	Bellazzini (2008)
$-4.05 \pm 0.02 \pm 0.10$	Tammann et al. (2008)
-4.01	Bono et al. (2008b)
-4.03[d]	Madore et al. (2009)
-4.02 ± 0.06[e]	Jang & Lee (2017)
-4.01 ± 0.04	Reid et al. (2019)
-3.97 ± 0.046	Yuan et al. (2019)
$-4.05 \pm 0.02 \pm 0.04$	Freedman et al. (2020)
$-4.04 \pm 0.01 \pm 0.03$[f]	Hoyt et al. (2021); LMC
$-4.05 \pm 0.03 \pm 0.04$[g]	Hoyt et al. (2021); SMC

Notes.
[a] At $(V-I) = 1.6$ mag unless otherwise noted.
[b] $-4.05 + 0.217 \times [(V-I) - 1.6]$.
[c] $-3.939 - 0.194 \times (V-I) + 0.08 \times (V-I)^2$.
[d] $-4.05 + 0.2 \times [(V-I) - 1.5]$.
[e] $-4.016 + 0.091 \times [(V-I)_0 - 1.5]^2 - 0.007 \times [(V-I)_0 - 1.5]$.
[f] 1.60 mag $< (V-I)_0 <$ 1.95 mag.
[g] 1.45 mag $< (V-I)_0 <$ 1.65 mag.

2. Absolute Calibration of the TRGB

As can be seen from Table 1, the value of the absolute *I*-band magnitude of the TRGB has remained quite stable over the 30 yr in which it has been measured, generally falling within the range of $M_I = -4.00$ to -4.05 mag (at $(V-I)_o = 1.6$ mag).

In this section, we present a summary of several independent calibrations of the TRGB that have become available since the Freedman et al. (2020) calibration, which was based solely on the DEB distance to the LMC. Importantly, these calibrations are based on very different methods for measuring absolute distances, including a geometric maser technique, geometric parallaxes, and geometric DEB distances. In Section 2.6, we combine all of these results to obtain an updated calibration of the TRGB. These results are summarized in Table 3 in Section 2.6.

2.1. The Megamaser Galaxy NGC 4258

The nearby spiral galaxy NGC 4258, at a distance of 7.6 Mpc, is an excellent target for providing a high-accuracy calibration of the TRGB. It is host to a sample of H_2O megamasers rotating within a highly inclined (87°) accretion disk about a supermassive black hole from which a geometric distance to the galaxy can be measured (see Humphreys et al. 2013; Reid et al. 2019). The most recent geometric distance to NGC 4258 is $\mu_0 = 29.397 \pm 0.024$ (stat) ± 0.022 (sys) mag (Reid et al. 2019), a 1.5% measurement.

The most extensive study of the TRGB in NGC 4258 was published by Jang et al. (2021). This measurement is based on a set of 15 archival HST/ACS fields covering 54 arcmin^2 located near the minor axis in the dust- and gas-free outer halo of the galaxy. The analysis was further confined primarily to regions at a deprojected semimajor axis distance of $>14'$ ($\sim$30 kpc) from the center of the galaxy. The RGB stars at this large distance are well separated from each other and demonstrably free from crowding/blending effects. Moreover, these halo RGB stars are relatively blue and metal-poor and do not exhibit a wide range in color/metallicity. The wide areal coverage results in a well-populated giant branch with about 3000 red giant stars 1 mag below the tip itself. As described in detail in Jang et al., extensive tests for systematics were undertaken, for example, using artificial stars, comparing DOLPHOT and DAOPHOT photometry, and comparing results using different point-spread functions, sky-fitting parameters, and radial spatial cuts. Moreover, the HST/ACS data used for this study are on the F814W flight magnitude system used in the F19 study and thus do not require a photometric transformation, as for the case of the LMC zero-point. Jang et al. obtained a TRGB zero-point of $M^{\rm TRGB}_{814} = -4.050 \pm 0.028 \pm 0.048$ using the maser distance determined by Reid et al. (2019). A detailed description of the error budget and the adopted statistical and systematic uncertainties are given in Section 6 and Table 4 of Jang et al. This independent TRGB calibration agrees to better than 1% with the value of $M_{814} = -4.054$ mag found earlier by F20, as well as that of -4.045 mag measured by Hoyt (2021), as described in Section 2.3.

Alternatively, if we instead determine the distance to NGC 4258 based on the LMC TRGB calibration of Hoyt (2021), given the measured apparent TRGB magnitude of $m^{N4258}_{814,o} = 25.347 \pm 0.014 \pm 0.005$ (Jang et al. 2021), we find a distance modulus of $\mu_o = 29.392 \pm 0.018 \pm 0.032$ mag. The agreement with the maser distance of 29.397 ± 0.033 mag (Reid et al. 2019) is at a level of better than 1%, differing by $<0.2\sigma$. In contrast, we note that a Cepheid calibration of the distance to NGC 4258 does not yield as good agreement with that of the maser distance. As recently described in Efstathiou (2020), a calibration of the Cepheid distance to NGC 4258 based on the LMC differs from the maser distance by 2.0σ–3.5σ, depending on the adopted correction for metallicity. The Milky Way and NGC 4258 metallicities are very similar, however, and should be independent of a metallicity effect. If instead, the Milky Way is adopted as the anchor galaxy to determine the Cepheid distance to NGC 4258, a distance modulus of 29.242 ± 0.052 is obtained, which differs from the maser distance by 7% at a 2σ level of significance. We defer a discussion of the implications of these differences to Section 5.

Finally, we note that the location of the fields studied by Jang et al. (2021) in the outer halo of NGC 4258 is optimal for avoiding dust and gas, as well as being separated from the high surface brightness galactic disk, thereby minimizing the level of systematic effects that plague efforts to measure the TRGB in the star-forming region of the disk of this galaxy, issues not considered, for example, in Macri et al. (2006) and Reid et al. (2019).

2.2. Galactic Globular Clusters

A second and completely independent method for calibrating the TRGB uses photometry of well-measured giant branches in globular clusters within our own Milky Way. Collectively, the Milky Way globular clusters span a wide range in metallicity, which overlaps well with those measured for giant stars in the halos of nearby resolved galaxies.

This approach to calibrating the TRGB was first carried out by Da Costa & Armandroff (1990) using CCD imaging data for six globular clusters. That calibration, for which distances were obtained using theoretical horizontal branch models from Lee et al. (1990; to calibrate the luminosities of RR Lyrae stars), formed the basis of the Lee et al. (1993) early application of the TRGB method to the extragalactic distance scale. A decade later, Ferraro et al. (1999) assembled a homogenous sample of

60 globular clusters, adopting the level of the theoretical zero-age horizontal branch as the basis from which to measure absolute distances. As these authors noted, the advantage of the horizontal branch is the simplicity of the measurement as compared to RR Lyrae stars, for which variability and evolutionary effects need to be accounted for and uncertainties due to metallicity still remain. Bellazzini et al. (2001, 2004) based their calibration on observations of the two populous globular clusters, ω Centauri and 47 Tucanae, calibrated using a DEB distance to ω Cen (Thompson et al. 2001), and an average of literature distances for 47 Tuc. Subsequently, Rizzi et al. (2007) based their distances on the well-developed horizontal branches of five Local Group galaxies (IC 1613, NGC 185, Fornax, Sculptor, and M33) spanning a range in metallicities of -1.74 dex $<$ [Fe/H] <-1.02 dex.

In a recent study, Cerny et al. (2020) analyzed a sample of 46 low-reddening ($E(B-V)<0.25$ mag) Milky Way globular clusters with uniformly reduced photometry available from Stetson et al. (2019) and through the Canadian Astronomy Data Center (CADC).[3] This 46-cluster catalog was then cross-matched to the Gaia Data Release 2 (DR2) database, and membership for these clusters was determined using the DR2 proper-motion data and a Gaussian mixture model clustering algorithm. Preliminary $E(B-V)$ reddening estimates and initial distance estimates were taken from Harris (1996, 2010).

A composite M_I versus $(V-I)_o$ CMD is shown in Figure 1 for the 46 low-reddening clusters from Cerny et al. (2020). This composite shows a well-defined giant branch, sampling a wide range of metallicities from -2.4 dex$<$ [Fe/H] <-1.0 dex. As described in more detail in Cerny et al., high signal-to-noise and low-extinction clusters were used to define a fiducial lower envelope to the blue and red horizontal branches, and a maximum-likelihood grid search technique was used to align the remaining clusters onto a common calibration. The zero-point of the calibration was set by the geometric DEB distance to ω Cen, measured by Thompson et al. (2001). The resultant blue and red horizontal branches are shown in Figure 1.[4] Applying a Sobel edge-detection filter to the composite luminosity function for the TRGB, Cerny et al. determined an absolute I-band TRGB magnitude of -4.056 mag, which, following F19, transforms to flight magnitudes as $M_{814W}=-4.063\pm0.022\pm0.101$ mag.

2.2.1. Gaia Early Data Release 3 Calibration of Galactic Globular Clusters

With the ESA Gaia mission, the promise of astrometry reaching tens of microarcseconds accuracy (Gaia Collaboration, Prusti et al. 2016) has been eagerly anticipated. Such astrometry for Galactic Cepheids, TRGB stars, and other distance indicators will ultimately fix the absolute zero-point of the extragalactic distance scale to an unprecedented accuracy of better than 1%. However, in early data releases, it was discovered that there is a zero-point offset (e.g., Lindegren et al. 2016). This offset results from the fact that the basic angle between the two Gaia telescopes is varying (resulting in a degeneracy with the absolute parallax). In addition, these variations lead to zero-point corrections that are a function of the magnitude, color, and position of the star on the sky (Arenou et al. 2018; Lindegren et al. 2018). In DR2, Arenou et al. (2018) and Mignard et al. (2018) found an average zero-point offset of -29 μas relative to the background reference frame for more than 550,000 quasars defined by the International Celestial Reference System.

Recently, the Gaia mission has released a new and updated database (Early Data Release 3; EDR3). This Gaia EDR3 database (Gaia Collaboration et al. 2021) contains parallaxes, proper motions, positions, and photometry for 1.8 billion sources brighter than magnitude $G=21$ mag (Lindegren et al. 2021b). The baseline for EDR3 is 34 months, compared to 22 months for DR2, and thus provides a significant improvement to the astrometry. The parallax improvement is estimated to be 20% compared to DR2; in addition, the variance in the parallaxes (the systematic uncertainty), as measured over the sky and estimated from quasars, has been reduced by 30%–40% (Gaia Collaboration et al. 2021). Still, on average, the zero-point offset for EDR3 is found to be -17 μas (in the sense that the Gaia parallaxes are too small). The Gaia collaboration has provided additional parallax corrections for EDR3, which are again a function of G magnitude, color, and ecliptic latitude (Lindegren et al. 2021a).

However, as the Gaia Collaboration emphasizes (e.g., Bailer-Jones et al. 2021; Fabricius et al. 2021), there is a significant variance in these measured offsets over the sky, and the EDR3 uncertainties in the parallaxes for different objects are correlated as a function of their angular separations. Lindegren et al. (2021a, 2021b) calculated the angular power spectrum of parallax systematic biases in Gaia EDR3 quasar data and estimated that the rms variation of the parallax systematics (excluding the global offset) is about 10 μas on angular scales $>\sim10°$. More recently, Maíz Apellániz et al. (2021) and Vasiliev & Baumgardt (2021) analyzed EDR3 parallax data for a sample of Milky Way globular clusters. Both studies concur with the result that there are significant rms variations on both large and small angular scales. Maíz Apellániz et al. concluded that the angular covariance limit results in a minimum (and systematic) uncertainty for EDR3 parallaxes for individual stars or small angular diameter clusters of 10.3 μas out to 30′. The rms fluctuations can reach as high as 30–50 μas. They further note that the uncertainty cannot be significantly reduced for larger clusters.

The minimum 10 μas systematic uncertainty in the EDR3 parallaxes limits the accuracy with which we can calibrate the TRGB for Galactic globular clusters. Cerny et al. (2020; as described in Section 2.2 above) based their calibration on the geometric DEB distance to ω Cen, anticipating that in future, accurate Gaia parallax measurements for all 46 clusters will be available for calibration. Object ω Cen has a measured Gaia EDR3 parallax of 189 μas or a distance of $5.25^{+0.28}_{-0.25}$ kpc (Maíz Apellániz et al. 2021; Vasiliev & Baumgardt 2021). Unfortunately, a minimum systematic uncertainty of 10 μas results in a minimum (large) distance uncertainty of 5% (0.1 mag) for ω Cen. Additionally concerning is that Vasiliev & Baumgardt provided evidence that the Gaia distances are systematically (and significantly) smaller than the previously published distances to these systems (the parallaxes are overestimated

[3] The Stetson catalog is based on a collection of about 90,000 images for 48 clusters, all having *UBVRI* photometry, for which a comparison of the different data sets constrains the photometric zero-point uncertainties at the millimag level. Eleven of those clusters did not meet the Cerny et al. (2020) low-reddening criterion. Cerny et al. expanded the Stetson catalog to incorporate nine additional low-reddening clusters with *BVI* photometry alone, archived at the CADC, and analyzed with the same DAOPHOT/ALLFRAME software (Stetson 1987, 1994).

[4] Note that the process of aligning the clusters based on their horizontal branches is completely independent of the TRGB.

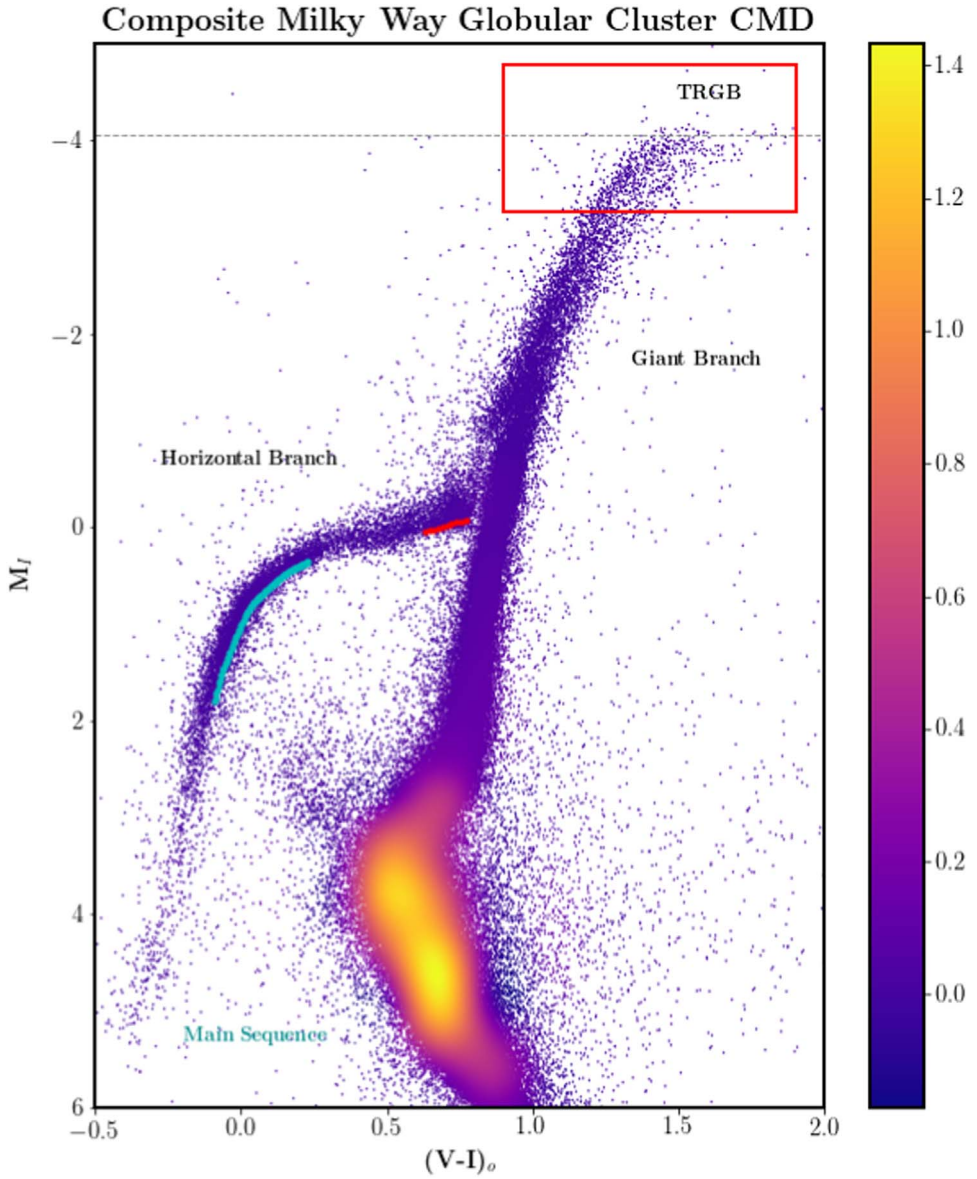

Figure 1. Composite M_I vs. $(V-I)_o$ CMD based on 46 Galactic globular clusters, color-coded by the density of the points. The clusters span a range in metallicity of -2.4 dex $<$ [Fe/H] < -1.0 dex. Cluster membership was determined from their Gaia DR2 proper motions. The red rectangular box outlines the region of the RGB that is expanded in Figure 9. The horizontal branch, main-sequence turnoff, and giant branch are labeled. The horizontal gray dashed line indicates the TRGB at $M_I = -4.056$ mag, and the cyan and red lines indicate the blue and red horizontal branch fits as measured by Cerny et al. (2020).

by 6–9 μas above the correction provided by Lindegren et al. 2021a).

Based on Gaia EDR3 measurements for ω Cen, Soltis et al. (2021) more optimistically quoted a parallax measurement of 0.191 ± 0.001 (statistical) ± 0.004 (systematic) mas (2.2% total uncertainty) corresponding to a distance of 5.24 ± 0.11 kpc, an uncertainty significantly smaller than (the minimum of 5%) demonstrated by all of the studies discussed above. As Vasiliev & Baumgardt (2021) noted, these rms variations across the sky are irreducible at present, and they thus conclude that the true uncertainty of the Soltis et al. result has been significantly underestimated.

Further independent constraints on the distance to ω Cen come from measurements of the RR Lyrae stars in the cluster. Recent near-infrared *JHK* measurements by Braga et al. (2018) result in distances of 5.43–5.49 kpc (depending on their metallicity calibration) with quoted total uncertainties of 2%, in good agreement with the DEB distance, as well as with a number of other published optical and near-infrared RR Lyrae measurements listed in their Table 8. To within the 1σ uncertainties, the recent RR Lyrae distance scale agrees with the Gaia EDR3 measurements of Maíz Apellániz et al. (2021) and Vasiliev & Baumgardt (2021).[5]

The uncertainties (of order 5%) in both the DEB and Gaia EDR3 distances for ω Cen are currently too large to provide the 1% level of accuracy that will ultimately be required for a resolution of the tension in H_0. For this paper, we adopt the Cerny et al. (2020) calibration, with a distance of 5.44 kpc, and its (large) associated uncertainty of $\pm 5\%$ (± 0.1 mag). As a

[5] More recently, Baumgardt & Vasiliev (2021) obtained a 1% distance to ω Cen by combining CMD fitting, RR Lyrae, and DEBs, in addition to the new Gaia EDR3 distance, corrected for the systematic offset. They found a distance of 5.426 ± 0.047 kpc (their Table 2), in excellent agreement with the results presented here.

result, it receives a lower weight in the determination of the value of H_0 described in Section 3. We note that adopting the Gaia EDR3 distance of 5.25 kpc with the same uncertainty of ±5% increases H_0 by only 0.1% in the final analysis.

The Gaia parallaxes and additional measurements will continue to improve as longer time baselines are established over the course of the mission; the full potential of Gaia has yet to be realized. The DR4 and DR5 are expected to be based on 5.5 and 10 yr of data, respectively.[6]

2.3. LMC Calibration

Using the OGLE "Shallow" survey data of Ulaczyk et al. (2012), F20 measured the TRGB for the LMC.[7] In order to avoid crowding/blending effects within the high surface brightness bar, the sample of stars analyzed was confined to stars outside of a circle of 1° radius, centered on the bar of the LMC. The LMC reddening and extinction were measured using *VIJHK* photometry, differentially with respect to two low-reddening galaxies, IC 1613 and the SMC. Based on the DEB (Pietrzyński 2019) distance modulus to the LMC of 18.477 mag, the extinction-corrected absolute magnitude of the TRGB for the I band was found to be $M_I^{\rm TRGB} = -4.047 \pm 0.022$ (stat) ± 0.039 (sys) mag. The Pietrzyński measurement is based on the surface brightness–color calibration for late-type giant stars, from which the angular diameters of giant stars can be measured to an accuracy of 0.8%.

Recently, Hoyt (2021) undertook a detailed remeasurement of the LMC TRGB based on OGLE-III photometry, isolating regions where the edge-detection measurements are sharp and single-peaked. He illustrated that these same regions are also low in dust content and located away from regions of star formation. He incorporated the new reddening and extinction maps of Skowron et al. (2021) determined from the colors of red clump stars based on OGLE-IV photometry. Adopting the 1% distance to the LMC based on DEBs (Pietrzyński 2019), he found $M_I^{\rm TRGB} = -4.038 \pm 0.012$ (stat) ± 0.032 (sys) mag, consistent to within 1% with the earlier results. A detailed description of the error budget and the adopted statistical and systematic uncertainties is given in his Table 3. The systematic uncertainty includes a ±0.01 mag term on the OGLE photometric zero-point. An additional ±0.01 mag systematic uncertainty is included in the ground-to-HST calibration, resulting in $M_{814}^{\rm TRGB} = -4.045 \pm 0.012 \pm 0.034$ mag.

As an aside, we note that Yuan et al. (2019) argued that the F19 calibration of H_0 based on the distance to the LMC was in error. However, Freedman et al. (2020) and Hoyt (2021) described in some detail a number of incorrect assumptions that were made by Yuan et al. The excellent agreement found here between the completely independent LMC, NGC 4258, SMC, and Galactic globular cluster calibrations argues even more strongly against the claims made in Yuan et al. Moreover, even if the LMC were to be excluded from the TRGB calibration altogether, the resulting change in the overall value of H_0 is insignificant (<1%).

2.4. The SMC

The interaction of the LMC and SMC has resulted in a tidally extended structure to the SMC, which has historically complicated the measurement of the SMC distance. The TRGB was measured by F20 using published OGLE data[8] for the inner region of the SMC, thereby avoiding confusion with the more extended tidal tails. They measured an I-band magnitude for the TRGB of $m_I^{\rm TRGB} = 14.93$ mag, adopting a foreground extinction value of $A_I = 0.056$ mag.[9]

Mapping out the inclined system with very high precision, Graczyk et al. (2020) recently measured a new DEB distance to the central region of the SMC to an accuracy of better than 2% based on the surface brightness–color calibration of Pietrzyński (2019). Augmenting the sample of measured DEBs from their previously published sample (from 5 to 15, a threefold increase), Graczyk et al. (2020) determined a distance modulus of $\mu_0 = 18.977 \pm 0.016$ (stat) ± 0.028 (sys) mag. The SMC thus provides another opportunity for an updated and independent calibration of the TRGB. An advantage of the SMC is its low star formation rate and dust content.

Hoyt (2021) undertook a reanalysis of the SMC OGLE-III data incorporating the updated Skowron et al. (2021) reddening maps. He measured an apparent tip magnitude of $m_I^{\rm TRGB} = 14.93$ mag. A detailed description of the adopted statistical and systematic uncertainties is given in his Table 3. Based on the new Graczyk et al. (2020) true DEB distance modulus, he found $M_I^{\rm TRGB} = -4.050 \pm 0.030$ (stat) ± 0.040 (sys) mag, in excellent agreement with the NGC 4258, Milky Way globular cluster, and LMC calibrations discussed above. An additional ±0.01 mag systematic uncertainty is included in the ground-to-HST calibration, resulting in $M_{814}^{\rm TRGB} = -4.057 \pm 0.030 \pm 0.040$ mag.

2.5. Additional Comparisons

In the cases described in this section, we do not use these systems to calibrate H_0 but rather note their excellent consistency with the other calibrations presented here, lending further confidence to the overall calibration of the TRGB.

Two recent studies of the Sculptor (Tran et al. 2021) and Fornax (Oakes et al. 2021) dwarf spheroidal companions to the Milky Way provide additional calibrations of the TRGB, constituting consistency checks on the geometric calibrations (for the LMC, the Milky Way, NGC 4258, and the SMC) described above. Wide-field Magellan IMACS VI data were obtained for each galaxy, from which the positions of the apparent TRGB and the horizontal branch were measured. Tran et al. measured an extinction-corrected value of the apparent TRGB I-band magnitude for Sculptor of $m_{I_o}^{\rm TRGB} = 15.487 \pm 0.057 \pm 0.014$ mag. For Fornax, Oakes et al. found $m_{I_o}^{\rm TRGB} = 16.75 \pm 0.03 \pm 0.01$ mag. Adopting the absolute calibration of the horizontal branch from Cerny et al. (2020), as described in Section 2.2 above and shown plotted in Figure 1, yields true distance moduli of $19.56 \pm 0.03 \pm 0.10$ and $20.79 \pm 0.02 \pm 0.10$ mag for Sculptor and Fornax, respectively. These measurements yield absolute I-band calibrations of the TRGB (based on the horizontal branch) of $-4.07 \pm 0.06 \pm 0.10$ and $-4.04 \pm 0.04 \pm 0.10$ mag, again in excellent agreement with the independent calibrations based on NGC 4258, the LMC, and the SMC.

[6] https://www.cosmos.esa.int/web/gaia/science-performance

[7] The LMC data are available at http://www.astrouw.edu.pl/ogle/ogle3/maps/.

[8] The SMC OGLE data are available at http://www.astrouw.edu.pl/ogle/ogle3/maps/.

[9] The value quoted in Freedman et al. (2020) is for the extinction-corrected $I_o^{\rm TRGB}$ and not the apparent magnitude as stated. Adopting the distance modulus based on five previously measured DEB measurements (which yielded a value of $\mu_0 = 18.965$ mag) would result in a zero-point calibration for the TRGB of $M_I^{\rm TRGB} = -4.035 \pm 0.03$ (stat) ± 0.05 (sys) mag.

Table 2
Data for LMC Clusters

Cluster	μ_o	$E(V-I)$	A_I
NGC 2005	18.58	0.139	0.170
NGC 2019	18.57	0.083	0.102
NGC 1754	18.87	0.125	0.153
NGC 1835	18.48	0.111	0.136

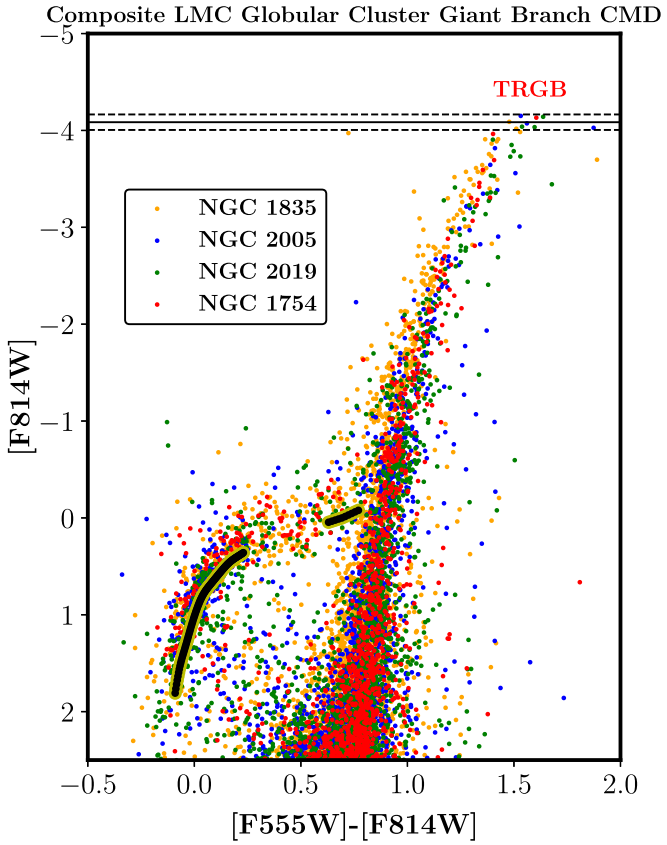

Figure 2. The I vs. $(V-I)$ CMDs for four LMC globular clusters based on HST/ACS data from Olsen et al. (1998). The blue and red fiducial horizontal branches defined by Cerny et al. (2020) are shown. The positions of the tip and 1σ uncertainties are illustrated by the solid and dashed horizontal lines at the top of the figure.

Finally, we have also examined the F814W and F555W HST/ACS data obtained by Olsen et al. (1998) for a number of globular clusters in the LMC, specifically, NGC 1754, NGC 1835, NGC 2005, and NGC 2019. Table 2 lists the reddenings and extinctions measured for each cluster by Olsen et al. and the true distance moduli based on the horizontal branch calibration of Cerny et al. (2020). We show a composite CMD for these objects in Figure 2. Adopting the Cerny et al. calibration results in a measured TRGB magnitude of $-4.085 \pm 0.05 \pm 0.10$ mag.

As noted previously, these systems are not of comparable accuracy (or independence) to yield an independent calibration of H_0, but their consistency, to within the uncertainties, already provides a further test of the robustness of the TRGB calibration. In future, when parallaxes accurate to 1% become available for a large sample of Milky Way globular clusters, these horizontal branch measurements will become a powerful independent route to a calibration of the TRGB.

Table 3
TRGB Zero-point Calibration

Object	$M_{\rm F814W}^{\rm TRGB}$ (mag)	$\sigma_{\rm stat}$	$\sigma_{\rm sys}$	References
NGC 4258[a]	−4.050	0.028	0.048	Jang et al. (2021)
Milky Way globular clusters[b]	−4.063[c]	0.022	0.101	Cerny et al. (2020)
LMC[d]	−4.045[c]	0.012	0.034	Hoyt et al. (2021)
SMC[e]	−4.057[c]	0.030	0.040	Hoyt et al. (2021)
Sculptor[f]	−4.08[c]	0.06	0.10	Tran et al. (2021)
Fornax[g]	−4.05[c]	0.04	0.10	Oakes et al. (2021)
LMC globular clusters[h]	−4.085	0.05	0.10	This paper
Adopted value (MW, NGC 4258, LMC, SMC)	−4.049	0.015	0.035	This paper (Section 2.6)

Notes.
[a] H_2O megamaser distance calibration.
[b] Optical data, Gaia proper-motion selection; ω Cen DEB calibration; $M_I = -4.056$ mag.
[c] Transformation to $M_{\rm F814W}^{\rm TRGB} = M_I - 0.0068$ mag following Freedman et al. (2019).
[d] LMC DEB calibration; $M_I = -4.038$ mag. An additional $\pm$ systematic uncertainty is included in the ground-to-HST calibration.
[e] SMC DEB calibration; $M_I = -4.050$ mag. An additional $\pm$ systematic uncertainty is included in the ground-to-HST calibration.
[f] ω Cen DEB calibration; $M_I = -4.07$ mag.
[g] ω Cen DEB calibration; $M_I = -4.04$ mag.
[h] ω Cen DEB calibration.

2.6. Adopted TRGB Calibration

Table 3 lists the TRGB absolute magnitude at F814W for the geometric calibrations described above. Where the calibration was carried out for ground-based data (as for the LMC, SMC, and Milky Way clusters), these have been transformed to the HST/ACS F814W flight magnitude system. The NGC 4258 calibration was carried out entirely with HST and is already on the F814W flight magnitude system. As discussed in F19 and F20, the transformation from the I band to F814W results in a zero-point that is brighter by −0.0068 mag. As can be seen from this table, the good agreement of the TRGB zero-point based on the calibrations for many anchors means that the adoption or rejection of a particular galaxy does not significantly impact the overall result.

Figure 3 shows the relative probability density functions (PDFs) for the absolute TRGB F814W magnitudes discussed in Section 2 above. Here we separate the contributions of the statistical and systematic errors in each case, so that the contribution of both types of uncertainties can be clearly seen. In Figure 3(a)), the widths of the Gaussians represent the individual statistical errors in each determination only, whereas the systematic uncertainties are illustrated separately by the error bars at the top of the plot (using the same color coding) for each object. Conversely, in Figure 3(b), the widths of the

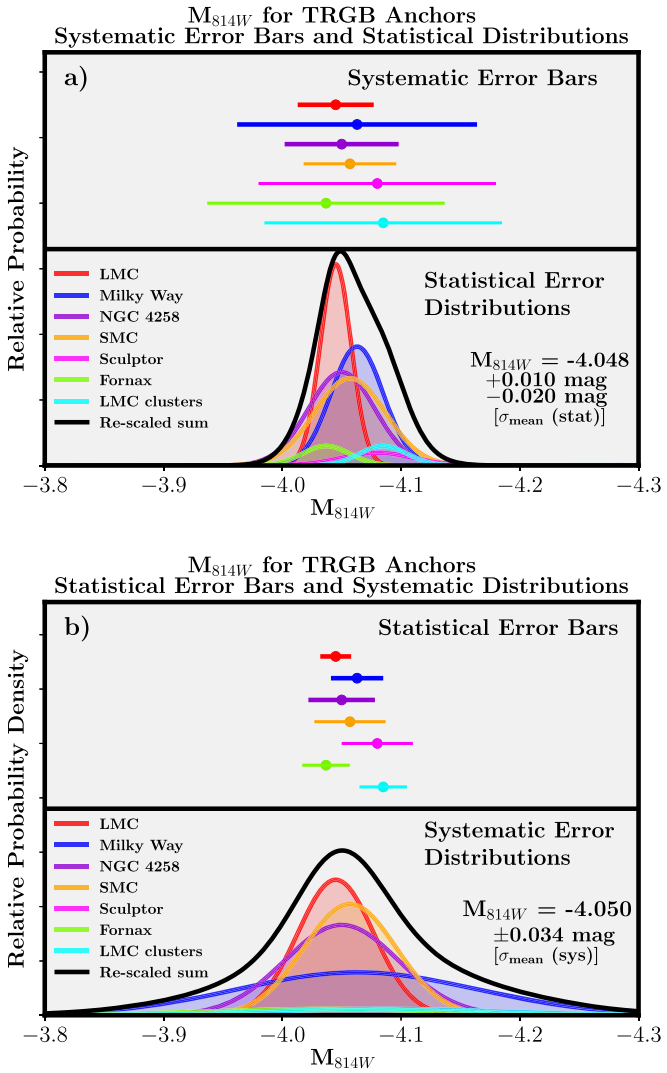

Figure 3. The PDFs for the measured absolute magnitude of the TRGB. The statistical and systematic errors are shown separately, so that the relative contributions of each can be easily seen for each galaxy. The statistical uncertainties can be improved by increasing the sample size in future, decreasing as $1/\sqrt{(N)}$. In Figure 3(a), the systematic error bars are shown at the top of the plot, and the statistical error distributions are shown at the bottom. In Figure 3(b), the statistical error bars are shown at the top, and the systematic error distributions are shown at the bottom. As discussed in Section 6.3, there is some covariance in the systematic uncertainties. Shown are the sum of all of the PDFs (black), the LMC (red), the Milky Way (blue), NGC 4258 (purple), the SMC (orange), Sculptor (magenta), Fornax (green), and the composite of the four LMC globular clusters (cyan). The results for Sculptor, Fornax, and the LMC clusters are shown for comparison purposes only. The statistical and systematic errors on the mean are labeled, along with the adopted value of $M^{\rm TRGB}_{\rm F814W} = -4.049 \pm 0.015$ (stat) $\pm$ 0.035 (sys) mag, consistent, to within 0.001 mag, with the mode of the summed distribution in each case.

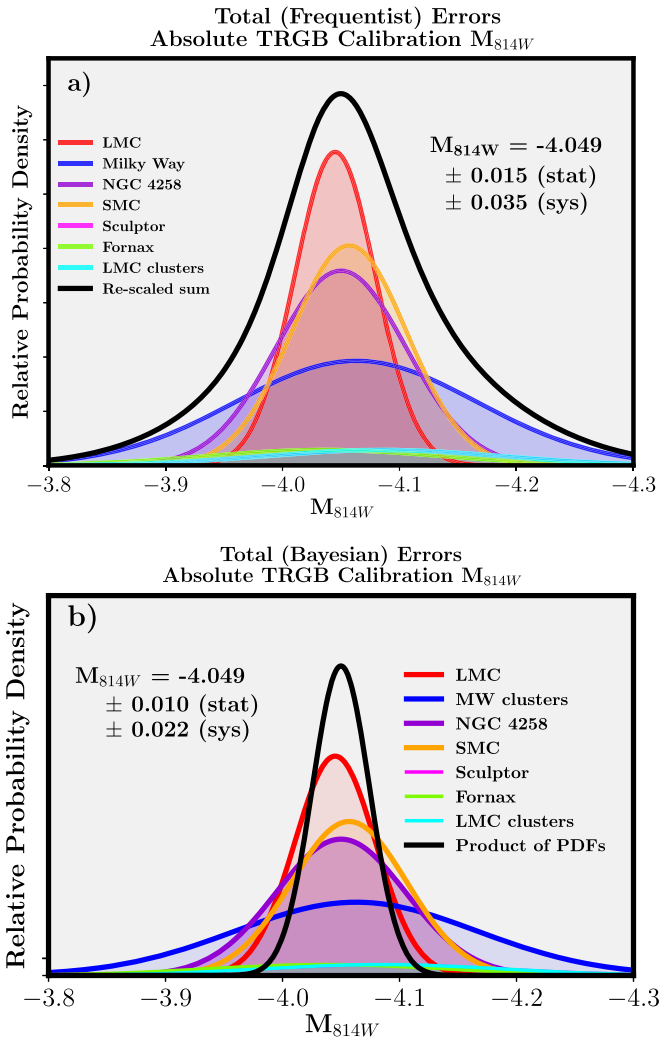

Figure 4. The PDFs for the measured absolute magnitude of the TRGB. The total errors (statistical and systematic, combined in quadrature) are shown, as described in the text. Figure 4(a) shows the frequentist sum of all of the PDFs (black), the LMC (red), the Milky Way (blue), NGC 4258 (purple), the SMC (orange), Sculptor (magenta), Fornax (green), and the composite of the four LMC globular clusters (cyan). The statistical and systematic errors on the mean are labeled, as described in the text, along with the adopted value of $M^{\rm TRGB}_{\rm F814W} = -4.049 \pm 0.015$ (stat) $\pm$ 0.035 (sys) mag. Figure 4(b) shows the product of the PDFs. The color scheme is the same as that for Figure 3.

PDFs represent the individual systematic errors in each determination only, whereas the statistical uncertainties are illustrated separately by the error bars at the top of the plot. The integrals of the PDFs for the LMC, the Milky Way, NGC 4258, and the SMC each have unit area. The statistical and systematic errors for each individual determination, σ_i, are given by the 16th and 84th percentiles of the Gaussians in Figures 3(a) and (b), respectively. The frequentist sums of the probability distributions are shown in both cases by the black lines. For the total sample, $\sigma_{\rm mean} = \sum \sigma_i / \sqrt{(N-1)}$, where $N = 4$.

As we have seen, the Milky Way TRGB magnitude is based on a sample of 46 clusters calibrated to the DEB distance to ω Cen. The calibrations of Sculptor, Fornax, and the LMC clusters are not independent, however, since they all rely on the Milky Way calibration of the horizontal branch. Moreover, Sculptor and Fornax are single objects, and the TRGB for the LMC clusters is sparsely populated. For illustrative purposes, in Figures 3(a) and (b), the areas for these Gaussians have thus been down-weighted by a factor *1/f*, as shown in Equation (1),

$$\frac{1}{f\sqrt{2\pi\sigma^2}} e^{-0.5\left(\frac{x-\langle x\rangle}{\sigma^2}\right)}, \quad (1)$$

where $f = \sqrt{(N)}$, and $N = 46$, the size of the Milky Way globular cluster sample. Thus, Sculptor, Fornax, and the LMC

Table 4
Values of H_0 (km s^{-1} Mpc^{-1}) for Various Choices of Fit

	Tripp				$E(B-V)$			
Band	H_0 (CSP18)[a]	σ	H_0 (CSP20)[b]	σ	H_0 (CSP18)[a]	σ	H_0 (CSP20)[b]	σ
				Full Sample				
B	69.48	1.39	69.88	1.25	70.75	1.32	71.50	1.29
H	69.13	1.35	70.48	1.23	69.36	1.46	70.33	1.41
				$s_{BV} > 0.5$ and $(B-V) < 0.5$				
B	69.38	1.36	69.57	1.24	69.39	1.04	70.04	1.05
H	68.80	1.34	70.00	1.25	68.47	1.44	69.47	1.42

Notes.
[a] CSP SN Ia host-galaxy mass corrections from Burns et al. (2018).
[b] CSP SN Ia host-galaxy mass corrections from Uddin et al. (2020).

clusters do not contribute to the adopted overall calibration, but they do provide a consistency check on the horizontal branch–to–TRGB distance scale.

The frequentist sums of the probability distributions are shown by the black lines in Figure 4(a). The mode of the summed distribution for the four primary TRGB calibrators is −4.049 mag. As shown in Figure 4(b), an identical result is obtained for a Bayesian analysis (albeit with smaller uncertainty), in which a uniform prior is adopted, and the product of the distributions is determined. In addition, a simple weighted average for the LMC, the Milky Way, NGC 4258, and the SMC also gives a result to within 0.001 mag of −4.049 mag. We adopt this robust value, $M_{\rm F814W}^{\rm TRGB} = -4.049 \pm 0.015\,({\rm stat}) \pm 0.035\,({\rm sys})$ mag, for the absolute magnitude of the TRGB. The (exact) agreement of the various means of combining the four calibrations lends confidence to the overall result; i.e., it is independent of the choice of statistical approach adopted to combine the results. Finally, we note that this value agrees to better than 1% with that given by F20, who found $M_{\rm F814W}^{\rm TRGB} = -4.054 \pm 0.022 \pm 0.039$ mag.

3. The Hubble Constant Based on the TRGB

3.1. New TRGB Calibration of H_0 Based on SNe Ia

We turn now to a determination of H_0 based on the TRGB calibration discussed in Section 2.6. This is an update of the calibration of H_0 presented in F19 and F20, applied to the CSP sample of 99 SNe Ia observed at high cadence and multiple wavelengths (Krisciunas et al. 2017). That measurement of H_0 was based on HST/ACS observations of the halos of 15 galaxies that were hosts to 18 SNe Ia. The measured absolute *I*-band magnitude of the TRGB from Freedman et al. (2020) was $M_{\rm F814W} = -4.054 \pm 0.022\,({\rm stat}) \pm 0.039\,({\rm sys})$ mag, tied to the geometric DEB distance modulus to the LMC from Pietrzyński (2019) of 18.477 mag. We now use four independent calibrations (NGC 4258 and the Milky Way, LMC, and SMC), superseding the single calibration based on the LMC alone.

To briefly summarize, in F19, the CSP analysis was undertaken with the SNooPy package (Burns et al. 2018), which characterizes the SN Ia light-curve shape using a color-stretch parameter, s_{BV}. Magnitudes were computed using two different approaches to the reddening, where

$$B' = B - P^1(s_{BV} - 1) - P^2(s_{BV} - 1)^2 - {\rm CT} - \alpha_M(\log_{10} M_*/M_\odot - M_0), \quad (2)$$

where P^1 is the linear coefficient and P^2 is the quadratic coefficient in $(s_{BV} - 1)$, B and V are the apparent k-corrected peak magnitudes, α_M is the slope of the correlation between peak luminosity and host stellar mass M_*, and CT denotes the color term for the two approaches. In the first case, ${\rm CT} = \beta(B-V)$, where a color coefficient β results in a reddening-free magnitude, an approach originally proposed by Tripp (1998). In the second approach, ${\rm CT} = R_B\,E(B-V)$, where R_B, the ratio of total-to-selective absorption, and the reddening, $E(B-V)$, are solved for explicitly using both optical and near-infrared colors for each SN Ia. Using the Markov Chain Monte Carlo (MCMC) fitter described in Burns et al. (2018) and F19, which uses the "No U-Turn Sampler" from the data-modeling language STAN (Carpenter et al. 2017), and solving for the parameters in Equation (2), the value of H_0 and its error was obtained using both approaches.

As described in Hoyt et al. (2021), two new galaxies with directly measured TRGB distances have been added to the Carnegie Chicago Hubble Project (CCHP) sample since F19 and F20. Object NGC 5643 is host to SN 2013aa and SN 2017cbv (Burns et al. 2020), and NGC 1404, a member of the Fornax cluster, is host to SN 2007on and SN 2011iv (Gall et al. 2018). Hoyt et al. (2021) found that SN 2007on appears to be significantly underluminous, and it is therefore excluded from the current analysis. In F19, the distance to NGC 1404 was taken to be the average value given by the two other Fornax galaxies in the CCHP sample, NGC 1316 and NGC 1365. In this paper, we adopt the new direct distance to NGC 1404 (Hoyt et al. 2021) for SN 2011iv and add the two additional SNe Ia in NGC 5643, augmenting the sample of 18 SNe Ia described in F19 to an updated sample of 19. All distances are calibrated adopting $M_{\rm F814W}^{\rm TRGB} = -4.049 \pm 0.015\,({\rm stat}) \pm 0.035\,({\rm sys})$ mag and used as new input to the MCMC analysis described in F19 (C. Burns 2021, private communication).

In Table 4, we give the values of H_0 and the uncertainties obtained adopting the new calibration of $M_{\rm F814W}^{\rm TRGB}$. Listed are H_0 values based on both the CSP *B* band and *H*-band SNe Ia magnitudes for different color and dust-reddening constraints. The uncertainties (for the SN Ia analysis alone) are determined from a diagonal covariance matrix with respect to the TRGB distances. Following F19, we present results applying both the Tripp and explicit $E(B-V)$ reddening corrections. In addition, we present the results adopting host-galaxy masses from Burns et al. (2018) originally used in F19, as well as those measured in the more recent study of Uddin et al. (2020). Figure 5 shows these results in flowchart form.

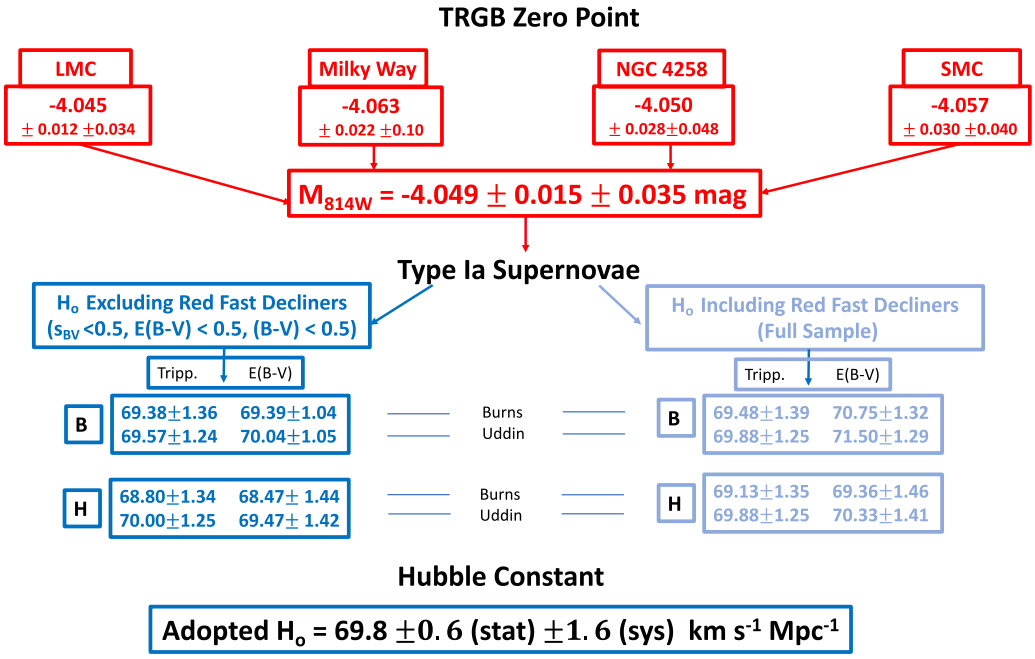

Figure 5. Overall flowchart summarizing the results of the TRGB zero-point calibration described in Section 2 and the SN Ia calibration described in Section 3, leading to the adopted value of $H_0 = 69.8 \pm 0.6$ (stat) $\pm$ 1.6 (sys) km s^{-1} Mpc^{-1}. The TRGB zero-point is based on the M_{814W} calibrations for the LMC, the SMC, NGC 4258, and the Milky Way. The adopted value of H_0 is based on a sample of SNe Ia restricted to those with $s_{BV} > 0.5$ and $(B-V) < 0.5$, for which there is good proportional overlap between the TRGB and more distant host-galaxy samples.

The values presented in Table 4 and Figure 5 represent different choices for the SN Ia sample (color and stretch), dealing with dust (Tripp versus $E(B-V)$), the bandpass for the SN Ia magnitudes (B versus H), and the host-galaxy mass peak SN Ia luminosity correlation (Burns versus Uddin). The various choices result in a full range in H_0 values from 68.47 to 71.50 km s^{-1} Mpc^{-1}. In selecting a best value of H_0 from those listed in Table 4, we select (following F19) the sample that minimizes the difference between the calibrator sample and the distant sample in terms of the nuisance variables: color, stretch, and host mass. In the histograms in Figure 6, we illustrate the characteristics of the SNe Ia in the distant galaxy sample compared with those for the TRGB calibrators. The TRGB sample is shown in green; the overall CSP sample is divided such that the blue, slow decliners (with $s_{BV} > 0.5$ and $(B-V) < 0.5$) are shown in blue (and labeled "slowblue") and those with fast decline rates and redder colors are shown in orange. In terms of stretch and color, the tails seen in orange (extending to $s_{BV} < 0.5$ and $(B-V) > 0.5$) are absent in the TRGB calibrating sample. Unambiguously, in terms of stretch and color, the sample with the best overlap of calibrator and distant SNe Ia is that of "slowblue." This sample also overlaps well in terms of host-galaxy mass, an advantage of the TRGB method, which can be applied to both early- and late-type galaxies. (Cepheid variables are young objects found only in star-forming, e.g., spiral, galaxies and cannot calibrate the SNe Ia found in elliptical or S0 galaxies.)

We note the following.

1. Using B-band photometry, restricting the sample to that with $s_{BV} > 0.5$ and $(B-V) < 0.5$ ("slowblue"), and basing the analysis on the more recent Uddin et al. (2020) host-galaxy masses results in a value of $H_0 = 69.57 \pm 1.24$ km s^{-1} Mpc^{-1} using the Tripp method and $H_0 = 70.04 \pm 1.05$ km s^{-1} Mpc^{-1} when explicitly correcting for dust ($E(B-V)$). Using H-band photometry, respectively, results in similar values of $H_0 = 70.00 \pm 1.25$ and 69.47 ± 1.42 km s^{-1} Mpc^{-1}. The corresponding values based on the Burns et al. (2018) masses are slightly lower. The difference arises primarily because the slope of the mass correlation in the optical is steeper for the Burns masses, whereas for the Uddin masses, the relation is nearly flat for all filters.
2. The H-band data have the advantage of a smaller dependence on the reddening, as the correction (R_λ) is smaller, but they have the disadvantage of a larger variance because the sample of SNe Ia having H-band photometry is smaller. (The "full sample" has 147 objects, "slowblue" restricts the sample to 129 objects, and restricting the sample to those with H-band photometry results in 102 objects.)
3. The largest value of H_0 (71.5) is obtained when the redder, faster decliners are included in the analysis (the "full sample"). However, as noted above, these solutions are strongly disfavored, since there are no redder, faster decliners in the more distant sample. In a broader context, no solution here reaches a value as high as 74 km s^{-1} Mpc^{-1}.

Although the differences in these H_0 values are small (a total range of only 3 km s^{-1} Mpc^{-1}), they illustrate the effect of different choices in the host-galaxy mass correlation and method/filters adopted to correct for dust.

Our adopted best-fit value is based on (1) the sample of SNe Ia for which the nuisance variables (color, stretch, and host mass) are comparable for the calibrating TRGB galaxies and the distant SNe Ia, (2) an average of the Tripp/$E(B-V)$ determinations, and (3) the recent host-galaxy masses measured by Uddin et al. (2020). We choose the B-band measurements because the sample of SNe Ia is largest, and the scatter for the

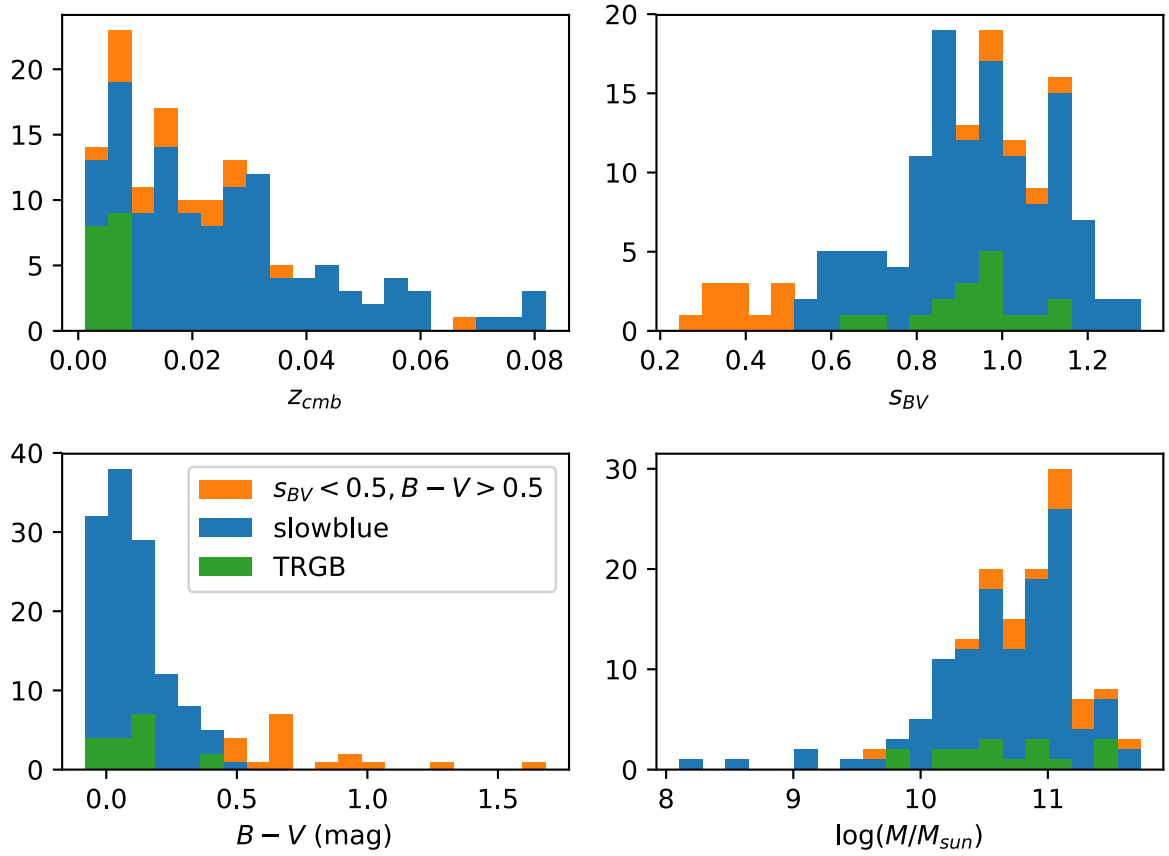

Figure 6. The upper left panel shows the redshift distribution for the total sample of CSP SNe Ia. In blue are the slow decliners (with $s_{BV} > 0.5$ and $(B-V) < 0.5$), labeled "slowblue." In orange are the red, fast decliners, and the nearby calibrating galaxies with measured TRGB distances are shown in green. The upper right panel shows the distribution of stretch values, and the lower two panels show the distributions of $(B-V)$ and $\log_{10}(\frac{M}{M_{\odot}})$. The "full sample" in Table 4 includes both the orange and blue distributions (i.e., the different samples are not overplotted, and no orange bins are being lost). The green TRGB distribution is well matched to that of the slower, bluer decliners and does not exhibit the extended tails seen in orange for the stretch (with $s_{BV} < 0.5$) and color ($(B-V) > 0.5$) of the red, fast decliners.

Table 5
H_0 Values for Common TRGB and Cepheid Calibrators

Calibrator	H_0 (TRGB)	H_0 (Cepheids)[a]	Cepheid References
LMC	69.9 ± 0.5 (stat) ± 1.6 (sys)	74.22 ± 1.82	Riess et al. (2019)
NGC 4258	69.7 ± 1.0 (stat) ± 2.0 (sys)	72.0 ± 1.9	Reid et al. (2019)
Milky Way	69.3 ± 0.8 (stat) ± 3.5 (sys)	73.0 ± 1.4	Riess et al. (2021)
SMC	69.5 ± 1.0 (stat) ± 1.7 (sys)	...	...
Adopted value	69.8 ± 0.6 (stat) ± 1.6 (sys)	73.2 ± 1.3	Riess et al. (2021)

Note.
[a] The published SHoES H_0 results are given with total errors only.

H-band measurements is 40% larger (or a factor of 2 in the variance, in the case of the $E(B-V)$ correction). We adopt a best-fit value of 69.8 ± 1.2 (sys) km s^{-1} Mpc^{-1}. This latter uncertainty takes into account the systematic uncertainties in the SN Ia analysis alone, without yet combining it with the TRGB zero-point systematic error. As discussed in Burns et al. (2018) and Freedman et al. (2019), all of the correction factors to the SN Ia light curves (P^1, P^2, $s_{BV}-1$, α_M, β, $E(B-V)$, R_B) as described in Section 2 are computed; these then provide corrected magnitudes and a full covariance matrix used to determine H_0 and the uncertainty given in Table 4. The total uncertainty adopted for H_0, including the uncertainty in the TRGB calibration, is discussed below.

Table 6
Summary of H_0 Uncertainties

Source of Error	Random Error	Systematic Error	Description
TRGB zero-point	0.7%	1.6%	Section 2.6
CSP-I SNe Ia	0.5%	1.7%	F19, Section 3
Total	0.9%	2.3%	In quadrature

The H_0 values and uncertainties based individually on the new TRGB calibrations for NGC 4258 (Section 2.1), Galactic globular clusters (Section 2.2), the SMC (Section 2.4), and the LMC (Section 2.3) are listed in Table 5. For comparison, also listed are the H_0 values, their uncertainties, and their published

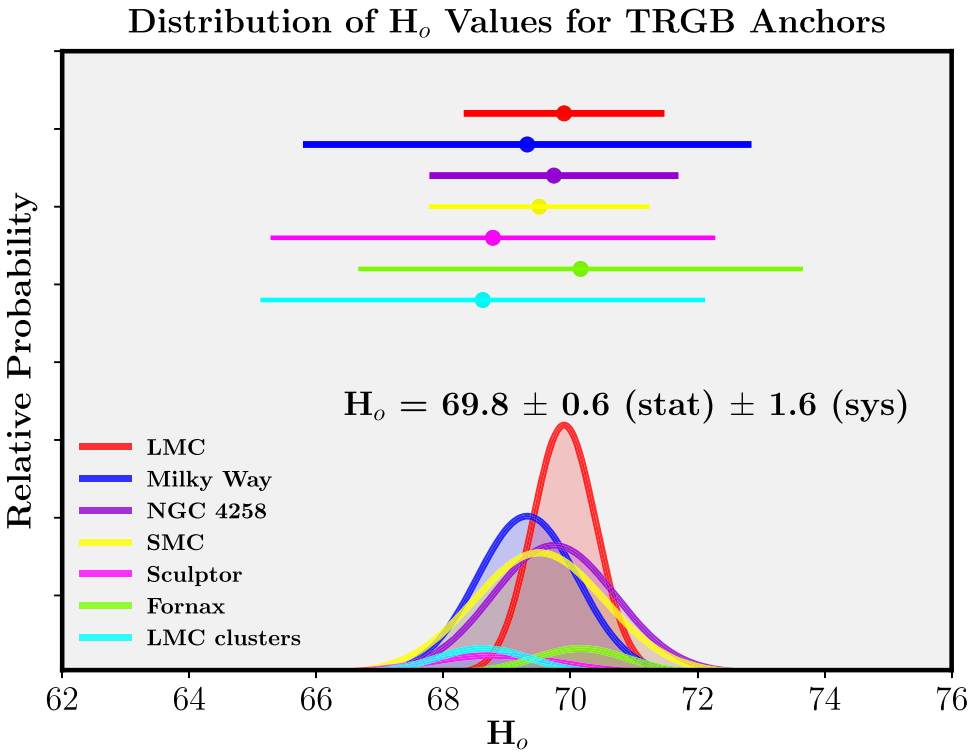

Figure 7. The PDFs for the values of H_0 based on the seven calibrations described in Section 2. The direct geometric calibrations for the LMC, the Milky Way, NGC 4258, and the SMC are independent of each other. The H_0 values for Sculptor, Fornax, and the four LMC clusters are based on the Milky Way calibration of the horizontal branch (and are therefore not completely independent). They are consistent with the direct geometric calibrations, but they are not included in the final calibration.

references from the SHoES team, based on the Cepheid calibrations for the LMC, NGC 4258, and the Milky Way.

Both statistical and systematic uncertainties are given for the TRGB H_0 determinations in Table 5. The error bars include both the uncertainties for the TRGB calibration discussed in Section 2.6 above and those arising from the calibration of the SNe Ia, as discussed above and in F19. For the SNe Ia, the statistical uncertainty amounts to $\pm 0.5\%$ with a systematic uncertainty of $\pm 1.7\%$. The final percentage errors are summarized in Table 6, with a final adopted value of $H_0 = 69.8 \pm 0.6$ (stat) $\pm$ 1.6 (sys) km s^{-1} Mpc^{-1}.

Figure 7 shows the PDFs for the values of H_0 based on the seven calibrations of the TRGB discussed in Section 2. The width of each Gaussian is based on the statistical uncertainties alone for each individual determination. The error bars at the top of the plot (using the same color coding) represent the corresponding systematic uncertainties in each case. The 1σ uncertainties are determined from the 16th and 84th percentiles for the frequentist sum of the distributions, adding the statistical and systematic errors in quadrature: $\sigma_i = \sqrt{{\sigma_{\mathrm{stat},i}}^2 + {\sigma_{\mathrm{sys},i}}^2}$ and $\sigma_{\mathrm{mean}} = \sum \sigma_i / \sqrt{(N-1)}$, where $N = 4$. The four objects with independent geometric distances (the LMC, the Milky Way, NGC 4258, and the SMC) are represented by Gaussians with unit area. The secondary calibrations of Sculptor, Fornax, and the LMC clusters are based on the Milky Way calibration of the horizontal branch and therefore not completely independent. Once again, their areas have been scaled following Equation (1) and are shown for illustrative purposes only. Thus, Sculptor, Fornax, and the LMC clusters do not contribute to the adopted overall calibration, but they do provide a consistency check on the horizontal branch–to–TRGB distance scale.

From Figure 7, it can also be seen that the range in the values of H_0 for the various calibrators is small relative to the published systematic error bars. The small χ^2 value may be indicating that the systematic errors have been overestimated or, alternatively, that statistical fluctuations have resulted in a fortuitously tight grouping of H_0 values. In either case, a conservative estimate of the overall uncertainty still seems warranted; that is, we do not consider this (better than 1% statistical) agreement to be indicating that H_0 has now been measured to a level of 1%.

In Figure 8, we show the normalized relative PDFs for the values of H_0 based on the different calibrators (the LMC, NGC 4258, the Milky Way, and the SMC), comparing both the TRGB and Cepheid calibrations in a self-consistent manner. For comparison with the SHoES results (where the statistical and systematic uncertainties are not treated independently), only the total uncertainties are considered. The TRGB calibrations are shown at the top (in red) and the Cepheid calibrations in the middle (in blue). In this case, we follow a Bayesian approach, assuming that each anchor is equally valid and adopting a uniform prior. The bottom panel shows the product of the PDFs. In the case of the Milky Way, the H_0 values are based on the calibration from Cerny et al. (2020) for the TRGB and R21 for the Cepheids. (The earlier Cepheid results for the Milky Way based on HST/WFC3 scanning parallaxes (R16) resulted in a much higher value of $H_0 = 76.18 \pm 2.17$ km s^{-1} Mpc^{-1}.) The resulting values of H_0 for the TRGB and Cepheids, respectively, are shown as solid lines. The difference between the TRGB calibration with $H_0 = 69.8 \pm 0.6$ (stat) $\pm$ 1.6 (sys) km s^{-1} Mpc^{-1} (this paper) and the Cepheid calibration with $H_0 = 73.2 \pm 1.3$ km s^{-1} Mpc^{-1}

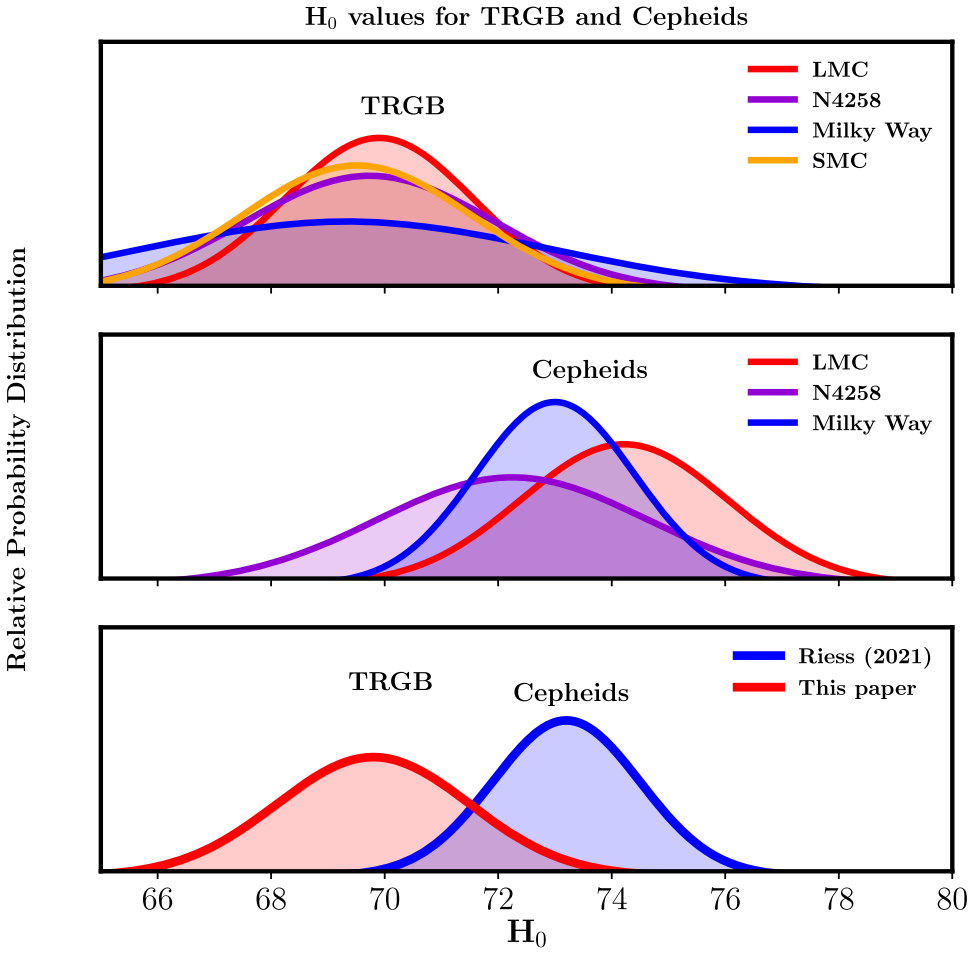

Figure 8. Comparison of the calibrations for the TRGB method and Cepheids, as listed in Table 5. In the upper two panels, PDFs are shown for the independent calibrations for each method: the LMC (red), NGC 4258 (purple), the Milky Way (blue), and the SMC (orange), in the case of the TRGB, and the LMC, NGC 4258, and the Milky Way in the case of Cepheids. The lower panel shows a comparison of the product of the PDFs for the TRGB method and the Cepheids based on the results from the upper panels. The TRGB results are shown in red; Cepheid results are shown in blue. Note that the relative weights of the TRGB and Cepheid distributions are determined, to a large extent, by the differing uncertainties adopted for the Milky Way calibrations, where the Cepheid result assumes a highly optimistic view of the current Gaia EDR3 calibration.

(R21) represents a 1.6σ tension between the TRGB and Cepheid calibrations.

The tension between the TRGB and Cepheid calibrations is perhaps not a serious problem, given that systematic uncertainties can be difficult to identify, and 2σ indicates generally good agreement, given those challenges. However, unlike the tension between the early universe (CMB results) and the local value of H_0, the true distances to galaxies are fixed with unique values. Rather than signifying potential new physics in the early universe, this "local" tension is unambiguously signaling that the uncertainties in one or both distance scales (out to and including the SNe Ia) have been underestimated.

4. Recent Independent Calibrations of the Cepheid Zero-point

4.1. Gaia EDR3 Calibration of the Leavitt Law

Gaia EDR3, as described in Section 2.2.1, also presents the opportunity to derive a new zero-point calibration for Milky Way Cepheids (e.g., R21; Breuval et al. 2021; Owens et al. 2021). (The R21 results were shown in the third panel of Figure 8.) We discuss the Owens et al. Gaia EDR3-based calibration of a multiwavelength sample of field Cepheids below and compare these calibrations with the sample of field Cepheids analyzed by R21.

Owens et al. (2021) analyzed Gaia EDR3 data for 49 Milky Way field Cepheids in an attempt to provide a multiwavelength calibration of the Leavitt law. In early anticipation of the Gaia mission, Freedman et al. (2011) and Monson et al. (2012) undertook a program to augment the sample of published optical photometry for Milky Way Cepheids with Spitzer mid-infrared (3.6 and 4.5 μm) photometry, providing a multi-wavelength (*BVRIJHK*[3.6][4.5]) database for 37 Cepheids, located both in the field and in open clusters.

Adopting the photogeometric distances obtained from the EDR3 parallax measurements by Bailer-Jones et al. (2021), Owens et al. (2021) derived optical–to–mid-infrared Leavitt law relations for the Milky Way sample. The Bailer-Jones et al. measurements include correction for the zero-point offset in Gaia EDR3 parallaxes (Lindegren et al. 2021a). A challenge at present is that this sample of Milky Way Cepheids is very bright in apparent magnitude ($4 \text{ mag} < G < 11$ mag). As already discussed in Section 2.2.1, the corrected Gaia EDR3 parallaxes have large uncertainties and have been shown to be underestimates. Moreover, they are significantly underestimated at brighter magnitudes (e.g., El-Badry et al. 2021), up to 30% for isolated sources with small quoted astrometric

uncertainties (and up to 80% for those with companions). It was found by R21 that a −14 μas correction to their Cepheid parallaxes was indicated, obtained by minimizing the scatter in their Wesenheit Leavitt law.

In a comparison with HST parallaxes and published infrared Baade–Wesselink distances, as well as the DEB distances to the LMC and SMC, Owens et al. (2021) concluded that the current uncertainty in their sample of EDR3 parallaxes is conservatively at a level of ∼±5%, much larger than the 1% or better accuracy anticipated from future (DR4 and DR5) Gaia releases. Owens et al. also explored adding a constant offset to the Leavitt law but found that there is no single offset that minimizes the scatter (as would be expected for distance errors) for their multiwavelength sample. They instead used the DEB distances measured for the LMC and SMC by Pietrzyński (2019) and Graczyk et al. (2020) to provide an external estimate of the offset in the Milky Way sample, finding a value of +17.5 μas, similar in magnitude but opposite in sign to that found by R21. (The sense of the offset found by Owens et al. is in the same sense as that found by Maíz Apellániz et al. (2021).) However, as Owens et al. emphasized, the adoption of the DEB distances does not then provide an independent Gaia EDR3 zero-point calibration, and uncertainty in the required correction to the Gaia EDR3 parallaxes remains.

Although the uncertainties are not yet at a level of 1%, there is still internal consistency at a few percent level in the Cepheid zero-points obtained using different Cepheid samples, parallax measurements, and external constraints and analyzed by different authors.

5. Comparison of the TRGB and Cepheid Calibrations of H_0

The adopted TRGB value of $H_0 = 69.8 \pm 0.6\,(\mathrm{stat}) \pm 1.6(\mathrm{sys})\ \mathrm{km\,s^{-1}\,Mpc^{-1}}$ is smaller than the most recent SHoES Cepheid calibration at a level of $\sim 2\sigma$. Next, we examine the implications of forcing a higher value of H_0 onto the calibration of the TRGB for globular clusters in the Milky Way.

Figure 9 shows an expanded version of the M_I versus $(V-I)_o$ CMD for the Milky Way globular clusters discussed in Section 2.2, this time centered on the giant branch. Corresponding values of H_0 are indicated. It can be seen that a value of $H_0 = 74\ \mathrm{km\,s^{-1}\,Mpc^{-1}}$ (R19) is significantly discrepant with the measured position of the TRGB, as are the values of $H_0 = 75$–$76\ \mathrm{km\,s^{-1}\,Mpc^{-1}}$ calibrated using scanning parallaxes for Milky Way Cepheids from R19, a recent calibration of the Tully–Fisher relation (Kourkchi et al. 2020), and surface brightness fluctuations (Verde et al. 2019). Values of H_0 of 74 and 76 $\mathrm{km\,s^{-1}\,Mpc^{-1}}$ correspond to adopting absolute magnitudes for the TRGB of $M_I = -3.92$ and −3.86 mag, respectively, significantly fainter than virtually all calibrations found in the published literature (see Table 1) and differing by 6% and 9% from the calibration adopted here. Future work is required to ascertain the reason for this discrepancy, most importantly, (1) further comparisons of individual TRGB and Cepheid distances to SN Ia host galaxies and (2) the ultimate establishment of the zero-point of both the TRGB and the Cepheid distance scales at a <1% level with future Gaia releases. For comparison, the Planck value of H_0 would correspond to adopting values of $M_I = -4.12$ mag (a 3% difference from our adopted calibration).

In Sections 2–4, we have seen that recent updates to the absolute zero-points of the TRGB and Cepheid distance scales are each internally consistent with previously published zero-points for each method at the 1%–2% level, and therefore that the difference in the values of H_0 based on these two methods cannot be (completely) ascribed to a zero-point error. A difference in H_0 of 4 $\mathrm{km\,s^{-1}\,Mpc^{-1}}$ (i.e., between 70 and 74 $\mathrm{km\,s^{-1}\,Mpc^{-1}}$) corresponds to a difference of 0.12 mag or 6% in distance, which is about three to six times the quoted uncertainty in the current estimates of the TRGB and Cepheid zero-points (of 1%–2%).

As discussed in F19, the TRGB and Cepheid distances to galaxies agree well (having a scatter of ±0.05 mag or 2% in distance) for nearby distances (<7 Mpc), but they begin to diverge for the more distant galaxies (where the scatter is more than three times larger, ±0.17 mag or 8% in distance), with a weighted average difference in distance modulus (in the sense of TRGB minus Cepheid; i.e., the TRGB distances are larger) amounting to +0.059 mag. Although in principle, one could adopt a TRGB zero-point that is significantly fainter than −4.05, that simply shifts the offset to (and worsens the good agreement at) closer distances where the current Cepheid and TRGB distances agree extremely well, with an average difference of +0.02 mag or 1% in distance.

One potential clue as to part of the problem may be indicated by the observed scatter in the calibrated absolute SN Ia magnitudes, as discussed by F19. These authors found that the scatter in the TRGB-calibrated SN Ia magnitudes for nearby galaxies amounted to $\sigma = 0.11$ mag, in good agreement with the scatter in the CSP Hubble diagram of $\sigma = 0.10$ mag for the more distant SN Ia sample, whereas the scatter in the Cepheid-calibrated SN Ia magnitudes is larger, with $\sigma = 0.15$ mag. Further improvement to the distances of galaxies in the 15–30 Mpc range will be needed to resolve this issue. Scheduled James Webb Space Telescope (JWST) observations will be critical to this effort (e.g., JWST Cycle 1 GO proposal 01995; Freedman et al. 2021).

Resolving the reason for this divergence is now critical to our understanding of whether there is new physics beyond the standard ΛCDM model.

6. The TRGB and Cepheids as Distance Indicators

Given the historical record of large and poorly understood disagreements among various distance indicators (for example, the 50 versus 100 discrepancy illustrated in Figure 9), the current (smaller) range of 67–74 in the value of H_0 also reflects the recent significant improvement in the extragalactic distance scale. That said, in the context of testing the standard cosmological model, it is essential to understand the origin of the difference in the TRGB and Cepheid distance scales.

We now turn to a discussion of each of the two methods individually. Specifically, we discuss the status of the calibrations, the viability of each method as a standard candle, the effects of crowding/blending for each case, and the uncertainties due to dust and metallicity. We highlight the particular strengths of each method, as well as the current level of control of known systematic effects, and then outline prospects for improvement.

6.1. Measuring TRGB Distances

1. *Calibration of the TRGB zero-point.* As shown in Section 2 of this paper, direct geometric calibrations of the TRGB method for the LMC (F19, F20; Hoyt 2021),

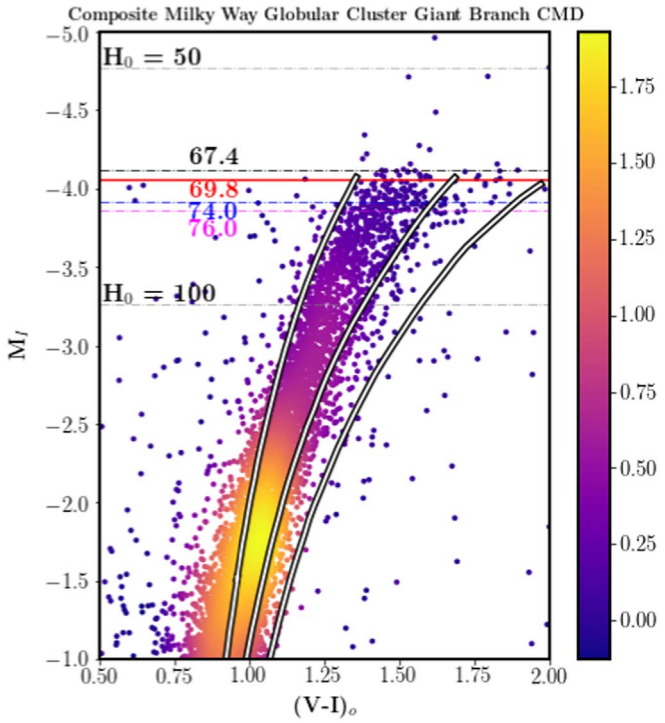

Figure 9. Composite M_I vs. $(V-I)_o$ CMD for giant branch stars, based on a sample of 46 Galactic globular clusters, color-coded by the density of the points. This plot is an expansion of the red rectangle shown in Figure 1. The TRGB is shown by the red line, located at an absolute I-band magnitude of $M_I = -4.049$ mag. This calibration results in a value of $H_o = 69.8$. Shown also for comparison as dash-dotted lines are the corresponding values for $H_0 = 67.4$, 74, and 76. Padova and Trieste Stellar Evolutionary Code (http://stev.oapd.inaf.it/cgi-bin/cmd) isochrones (CMD version 3.3; Bressan et al. 2012; Marigo et al. 2017) with [Fe/H] values from left to right of −2.0, −1.2, and −0.8 dex are illustrated by the three white curves outlined in black. The fits to these isochrones illustrate, both empirically and theoretically, how small the effect of metallicity is for the TRGB in the I band at these low metallicities. The historical H_0 values of 100 and 50 are also labeled; their large spread relative to current measurements illustrates the dramatic progress in the measurement of H_0 in recent decades.

NGC 4258 (Jang et al. 2021), the globular clusters in the Milky Way (Cerny et al. 2020; Freedman et al. 2020), and the SMC (Hoyt 2021) all agree to within ±1%.

2. *The TRGB as a standard candle*. The strikingly sharp and flat definition of the TRGB at F814W (comparable to the ground-based I band) for Milky Way globular clusters (see Figure 9) provides growing direct evidence that old, blue, metal-poor giant branch stars at the TRGB are actual standard candles, distinctive from other commonly employed standardizable candles (for example, SNe Ia and Cepheids). The fact that this sharp cutoff is not simply an empirical feature but rather the result of a well-understood physical mechanism (the core helium flash) lends confidence to the use of these stars as reliable distance indicators.
3. *Photometric errors due to crowding/blending effects*. The TRGB method is best applied in the outer halos of galaxies (e.g., see the discussion in Jang et al. 2021, and references therein), where the surface brightness of the galaxy is low and the overlapping of stellar point-spread functions is minimal. Crowding/blending effects are not currently a significant source of uncertainty for the TRGB method if carefully applied to stars in the outer halos of galaxies.
4. *Effects of dust: foreground and internal*. Foreground Milky Way reddening corrections are obtained from the all-sky extinction maps of Schlafly & Finkbeiner (2011). Beyond the Milky Way, for the application of the TRGB method targeted in the halos of galaxies, the effects of dust are small (e.g., Ménard et al. 2010). For the four current anchors (the LMC, the Milky Way, NGC 4258, and the SMC), the local line-of-sight circumstances are different for each case, and extinction and reddening corrections have been investigated in detail on a case-by-case basis as described in Jang et al. (2018), Cerny et al. (2020), Freedman et al. (2020), and Hoyt (2021). For an individual anchor, the distance uncertainty attributed to this correction contributes to its systematic uncertainty; however, for the determination of H_0 based on several anchors, it contributes only to the overall statistical error, and not to the final systematic uncertainty.
5. *Metallicity effects*. For RGB stars, there is a metallicity (and concomitant color) dependence of the luminosity that is both predicted by theory and independently confirmed by observation (e.g., Freedman et al. 2020). A significant advantage of the TRGB method is that it has long been known that the color of a star on the RGB is a direct indicator of the metallicity of the star (e.g., Da Costa & Armandroff 1990; Carretta & Bragaglia 1998).

   Given a known (flat) TRGB slope in the I band, the corresponding slope of the giant branch luminosity with color, at any other given wavelength, is not arbitrary; it is a priori mathematically defined for the other wavelengths (Madore & Freedman 2020). Empirically, the slope and zero-points of the *VIJHK* RGB terminations determined for the LMC and SMC agree with those measured for Milky Way globular clusters to within their 1σ uncertainties (F20; Cerny et al. 2020).

   For the purposes of the I-band (F814W) calibration presented in this paper, the effects of metallicity are negligible, given that only the bluest (metal-poor) stars enter the calibration, and that the flat (color-independent) nature of the TRGB in this restricted color regime is well established (see, for example, Figure 9 above and Figure 6 of Jang et al. 2021).
6. *Future prospects for the TRGB distance scale*.
   (a) *Strengthening the zero-point calibration*. In the future, Gaia DR4 will provide twice as many observations compared to EDR3 and a new full-scale astrometric solution with a decrease in both the random and systematic uncertainties (Lindegren et al. 2021a) compared to those discussed in Section 2.2.1 for EDR3.
   (b) *Increasing the number of SN Ia calibrators*.
      (i) As new SNe Ia are detected in galaxies at distances $\leqslant$30 Mpc, HST observations of the halos of the host galaxies can provide I-band TRGB distances with precisions of better than 2% for a modest investment in telescope time. Unique in this regard is that the method can be applied to galaxies of all types, including edge-on spiral, S0, and elliptical galaxies, thus both increasing the number of calibrators and also mitigating potential systematics in the SN Ia data.
      (ii) A combination of ground- and space-based observations can further strengthen the calibration

of the TRGB at other (near- or mid-) infrared wavelengths (e.g., Dalcanton et al. 2012; Hoyt et al. 2018; Madore et al. 2018; Durbin et al. 2020). Red giant stars are brighter in the near-infrared than at optical wavelengths. With JWST, the mid-infrared TRGB calibration can be applied to distances of $\gtrapprox$40 Mpc (or a volume five times greater than currently possible with HST), thereby adding significantly more SNe Ia into the calibration.[10]

6.2. Measuring Cepheid Distances

1. *Calibration of the Cepheid zero-point*. Direct geometric calibrations of the Cepheid Leavitt law for the LMC are based on (a) the DEB distance to the LMC (Pietrzyński 2019), (b) HST and Gaia parallaxes for field Cepheids in the Milky Way (Benedict et al. 2007; Riess et al. 2018, 2021), and (c) the maser distance to NGC 4258 (Reid et al. 2019). The resulting values of H_0 for these three calibration methods currently span a range of 72–74 $\mathrm{km\,s^{-1}\,Mpc^{-1}}$.[11]
2. *Cepheids as standardizable candles*. The well-defined relationship between period, luminosity, and color can, in principle, produce a standardizable candle of high precision. Then, including a metallicity term, the Leavitt law can be expressed as

$$M_{\lambda_1} = \alpha \log P + \beta(m_{\lambda_1} - m_{\lambda_2})_o + \gamma[\mathrm{O/H}] + \delta, \quad (3)$$

where the Cepheid magnitude at a given wavelength λ_1 is a function of the logarithm of the period (P), a color term with coefficient β, and a term with coefficient γ that allows for a metallicity effect (where [O/H] represents the logarithmic oxygen-to-hydrogen ratio for H II regions in the vicinity of the Cepheids relative to the solar value), and δ is the zero-point.

It has long been recognized that the decreasing scatter in the correlation between period and luminosity with increasing wavelength (e.g., Madore & Freedman 1991), as well as the decreasing effect of reddening and metallicity with increasing wavelength, motivates the application of the Leavitt law at near-infrared (or longer) wavelengths (McGonegal et al. 1982; Freedman et al. 1991, 2008; Madore & Freedman 1991; Macri et al. 2001).[12]

3. *Photometric errors due to crowding/blending effects*. Cepheid variables are yellow supergiants, generally found in relatively high surface brightness areas in the star-forming disks of late-type galaxies. For nearby galaxies, the crowding and blending of Cepheids is not a serious practical issue for the brightest long-period Cepheids, but the problem worsens as the distance increases and the angular resolution decreases. Using artificial star tests, R16 concluded that these crowding/blending effects do not induce systematic effects. In addition, Riess et al. (2020) tried to infer the quantitative effects of crowding by comparing the amplitudes of Cepheids in four galaxies out to a distance of 20 Mpc. They concluded that the erroneous measurements of Cepheid backgrounds alone cannot explain the Hubble tension. Future work is still needed to assess the implications for the even more distant galaxies in the SHoES program, which extend out to 40–50 Mpc.

The effects of crowding/blending also become more severe with increasing wavelength, where, for a given aperture telescope, the resolution is poorer in the infrared than in the optical. Disk red giants and the even brighter asymptotic giant branch (AGB) stars (both of which are redder than Cepheids) are the main, and unavoidable, contaminants. Thus, although both dust and metallicity effects are decreasing functions of wavelength, there is a trade-off to be made with the decreasing (wavelength-dependent) resolution and the increasing challenges of overlapping images dominated by red stars, particularly as the distance increases. In the case of HST and WFC3, the longest wavelength available, the F160W filter (comparable to the ground-based H band), has an advantage in reducing the effects of dust and metallicity, but it is at a disadvantage in dealing with the effects of increased crowding and blending.

4. *Effects of dust*. As a consequence of their relative youth, Cepheid variables are unavoidably located close to the regions of dust and gas out of which they formed. In practice, however, Cepheid reddening can be dealt with in a straightforward manner. With accurate colors, Madore (1976, 1982) showed that a reddening-free magnitude can be constructed; for example,

$$W = V - R_V \times (B - V), \quad (4)$$

where $R_V = A_V/E(B-V)$ is the ratio of total-to-selective absorption, and W has been widely applied to the Cepheid distance scale (e.g., Freedman et al. 2001; Riess et al. 2016). An advantage of W is that it simultaneously corrects for all line-of-sight absorption, including both host-galaxy (internal) and Galactic (foreground) reddening.[13]

5. *Metallicity effects*. The effects of metallicity on the Cepheid Leavitt law are still being actively debated in the literature (e.g., for a recent summary, see Ripepi et al. 2020). One of the immediate challenges in constraining any metallicity effect for Cepheids is the difficulty of determining abundances for the individual Cepheids themselves. Spectroscopic abundances have been measured for Cepheids in the Milky Way and LMC (e.g., Romaniello et al. 2008); however, more distant Cepheids are generally too faint to measure abundances from spectroscopy.

Three decades of empirical tests for a Cepheid abundance effect (the measurement of γ in Equation (3); e.g., Freedman & Madore 1990; Kennicutt et al. 1998; Romaniello et al. 2008; Fausnaugh et al. 2015; Riess et al. 2016; Ripepi et al. 2020; Breuval et al. 2021) have not yet led to a consensus view on the magnitude of the

[10] This new JWST capability is highly desirable because SNe Ia are sufficiently rare that host galaxies for which TRGB stars (or Cepheids) are also accessible with HST are discovered only every 1.5–2 yr.

[11] Efstathiou (2020) discussed at some length the internal tension between the LMC and NGC 4258 anchor distances (which depend upon the adopted metallicity correction) and noted that the H_0 tension may be arising, in part, due to inconsistencies in the local anchors.

[12] An exception is the 4.5 μm band, in which the Cepheid flux is affected by the presence of a CO bandhead (Scowcroft et al. 2011).

[13] As noted recently by Mortsell et al. (2021); however, if the assumption of a universal value for R_V is not valid, it could result in a systematic error in H_0, an issue that could become increasingly important in an era for which the goal is percent-level accuracy.

effect or even its sign, or indeed, whether there is an effect at any given wavelength. Most of these studies have had to rely on the use of [O/H] abundances for nearby H II regions as a proxy for the Cepheid metallicities, which cannot generally be measured directly. Theoretical models suggest that the effect of metallicity will be smaller at longer wavelengths, but there also remain significant differences in the predicted effects on both the slope and intercept of the period–luminosity relations with wavelength (Bono et al. 2008a; Ripepi et al. 2020), even at the long wavelength of the K band (2.2 μm). Ripepi et al. found that the slope of the metallicity term ranges from -0.04 to -0.36 mag dex^{-1} for fundamental pulsators and $+0.23$ to -0.30 mag dex^{-1} for overtone Cepheids. Recently, incorporating Gaia EDR3 data for the Milky Way and comparing to the LMC and SMC, Breuval et al. (2021) found that the metallicity effect is negligible in the optical (V band) and moreover, contrary to previous studies, concluded that the effect increases through $IJHK$, with the largest effect being in the near-infrared.

As we enter an era where 1%–2% accuracies are required to resolve whether there is an H_0 tension, it is critical that the long-standing uncertainties due to metallicity be better understood and calibrated. Authors R16 computed a Wesenheit function of the form

$$M_H^W = m_H - R_{H,VI} \times (V - I),$$
$$\text{where } R \equiv A_H/(A_V - A_I), \quad (5)$$

and solved for a metallicity correction on a star-by-star basis. Their conclusion is that metallicity contributes to their total H_0 uncertainty of 2.4% only at the 0.5% level. Given the long-standing disagreement in the literature (from both theory and observations), further work is clearly warranted to confirm this assertion. This issue is best addressed with multiwavelength, high signal-to-noise data for nearby galaxies where covariant crowding effects are less severe.

6. *Summary and future prospects for the Cepheid distance scale*. Cepheids have many strengths that make them good distance indicators. However, they still face a number of challenges, particularly when it comes to applying them under conditions at the limits of current telescopes and detectors, with the goal of achieving distances that are accurate and precise to a level of 1%–2%. The main challenge for Cepheid standardization is that several wavelengths, each of equally high precision, are required: first, to correct for reddening; second, to correct for a possible metallicity effect (the wavelength dependence and sign of which remain under debate); and third, to ensure that the effects of crowding/blending are not systematically influencing the results.

All three of the above systematic effects (reddening, metallicity, and crowding) increase toward the centers of galaxies. Since Cepheids are being crowded/blended, particularly by red giant and red (even brighter) AGB stars, all three effects will also act in the sense of causing Cepheids to appear redder in regions of coincidentally higher metallicity. Put another way, the corrections for reddening, metallicity, and crowding/blending are covariant; for example, if the currently applied metallicity or crowding corrections are incorrect, then the reddening corrections will also be in error because they all involve the same limited sets of colors, making it difficult to break the degeneracy. These issues will continue to pose a serious challenge for 1% accuracy, especially when the scatter in the observed Wesenheit Leavitt law can be 20%–25% in distance or 0.4–0.5 mag in distance modulus (R16), even for (anchor) galaxies as close as 7.6 Mpc (e.g., NGC 4258).

There are many areas where future tests could further constrain the uncertainties in the Cepheid distance scale.

(a) High signal-to-noise, multicolor, time-averaged ($BVIJHK$) photometry and spectroscopy for nearby galaxies with a range of metallicities can help resolve the question of the magnitude, sense, and wavelength dependence of metallicity corrections. The inclusion of additional distant galaxies will not lead to better constraints on the systematic effects, such as metallicity; obtaining larger samples of galaxies will simply reduce the statistical uncertainties alone.

(b) As further SNe Ia are discovered in the nearby universe, the numbers of SN Ia host galaxies with observable Cepheids will also slowly be increased.

(c) The JWST/NIRCam in the J band has four times the angular resolution of HST/WFC3 in the H band, where the longest-wavelength SHoES Cepheid measurements have been made, and thus can allow the effects of crowding/blending in the HST photometry to be assessed directly.

Table 7
Zero-point Calibration

Calibrator	TRGB	Cepheids
LMC	DEB[a]	DEB[a]
NGC 4258	Masers[b]	Masers[b]
Milky Way	ω Cen DEB[c]	EDR3 parallaxes[d]
SMC	DEB[e]	…

Notes.
[a] Pietrzyński (2019).
[b] Reid et al. (2019).
[c] Thompson et al. (2001).
[d] Riess et al. (2021).
[e] Graczyk et al. (2020).

6.3. Overall Systematics

At present, the systematic accuracies of the TRGB and the Cepheid distance scale zero-points are constrained by the small number of available geometric calibrators providing high-accuracy distances. Below, we outline the degree to which the two distance scales are codependent (or not) on the same (or different) zero-point calibrators.

As illustrated in Table 7, there are four galaxies with geometric measurements that have been used to calibrate the local distance scale: the LMC, NGC 4258, the Milky Way, and the SMC. There are several important points to take away from this table.

1. Both the TRGB and the Cepheids adopt the same distances for the LMC and NGC 4258, therefore sharing any systematic errors that may have been incurred in those measurements. The current total uncertainties

quoted for these measurements are at a level of 1% and 1.5%, respectively (Pietrzyński 2019; Reid et al. 2019).
2. The only galaxy sufficiently nearby for which an accurate maser distance can be measured is NGC 4258, which is also close enough for the calibration of the TRGB and Cepheids. A "sample of one" precludes rigorous testing for potential systematic errors in this galaxy's geometric distance.
3. In the case of the TRGB method, the LMC and SMC calibrations share the systematic uncertainties of the Skowron et al. (2021) reddening maps. The dominant uncertainty is that of the zero-point, estimated by Hoyt et al. (2021) to be ±0.014 mag (0.6%) and ±0.018 mag (0.8%), respectively. In addition, their DEB distances are both based on the surface brightness–color relation from Pietrzyński (2019), estimated to be 0.8%.
4. Finally, it should be noted that for both the TRGB and the Cepheids, the same reddening law is adopted and assumed to be universal; moreover, the same ratio of total-to-selective absorption, R_V, is adopted in both applications. However, the TRGB method is less susceptible to the assumption of the universality of the reddening law because the dust content in the halos of galaxies is generally negligible compared to that in the disks.

6.3.1. The SN Ia Host Galaxies

The tie-in to the more distant SN Ia host galaxies is similarly limited by the fact that SNe Ia in the local universe are rare. As noted previously, there are 19 SNIa calibrators for both Cepheids and the TRGB, and a sample of 10 galaxies for which there is an overlap. Any peculiarities in the SNe Ia in this overlap sample (that are not shared by the more distant SNe in the Hubble flow) will carry covariant systematics into the TRGB and Cepheid H_0 determinations.

Once again, the same reddening law is adopted for both the TRGB and Cepheids. It is assumed to be universal, and the same value or R_V is adopted in both applications. However, the explicit Galactic foreground reddening corrections used for the TRGB are decoupled from the Cepheid dereddening process that implicitly corrects for total line-of-sight reddening using the Wesenheit method.

6.3.2. Distant SNe Ia in the Hubble Flow

Both the TRGB and the Cepheids tie in to more distant SNe Ia in the Hubble flow for the final step in the determination of H_0. While different filters, software analysis tools, and groups have analyzed the data, any unknown systematics in SN Ia distances will be shared by both methods. However, the TRGB method, which can be applied to both elliptical and spiral galaxies, will be less sensitive to correlations that are host-galaxy mass-dependent.

As the distances to more SN Ia host galaxies are measured using HST and JWST, the statistical (uncorrelated) errors will decrease as $1/\sqrt{(N)}$. As the above discussion makes clear, however, there are parts of the systematic error budgets for the TRGB and Cepheid H_0 determinations that are covariant. Unfortunately, quantifying these potential covariant effects (many of which fall into the category of current unknowns, e.g., reddening laws, unknown systematics in masers, DEBs, SNe Ia, etc.) is not a realistic prospect. Ultimately, completely independent methods (e.g., gravitational-wave sirens) will be required to test for and place external constraints on covariant systematics in the local distance scale.

7. Comparison with Other Recent Determinations of H_0

To date, only 10 SNe Ia host galaxies have both TRGB and Cepheid distances measured (F19). Yet this sample is significantly larger than that available for any other primary distance indicator. Stated another way, this is the first independent and direct test for individual galaxies in the Cepheid–SNe distance scale, and significant differences between the TRGB and Cepheid distances have been found. What about other tests?

Although a case has been made that there are many independent checks of the Cepheid distance scale (e.g., Verde et al. 2019), the small number of galaxies currently available precludes a detailed and direct comparison of the Cepheid distance scale with most other distance indicators. For example, the Mira method (Huang et al. 2018) is currently based upon the detection of these long-period variable stars in a single galaxy, NGC 4258, calibrated via masers in that galaxy. Furthermore, the calibration of H_0 using this method then relies on observations of a single SN Ia host galaxy, NGC 1559 (Huang et al. 2020).

Similarly, NGC 4258, at a distance of 7.6 Mpc, is the only galaxy in the nearby universe where the host is close enough to have a measured Cepheid distance where the maser technique can also be applied (Reid et al. 2019). Furthermore, there are only six galaxies in total (including NGC 4258) for which maser distances have been measured and used to estimate H_0 (Pesce et al. 2020); the statistical errors for this technique are thus still large compared with, for example, SNe Ia (Burns et al. 2018; Scolnic et al. 2018), where samples of 100 or hundreds of SNe Ia have been measured. The five additional megamaser galaxies beyond NGC 4258 have distances ranging from 50 to 130 Mpc (with recession velocities of 680–10,200 km s^{-1}), and peculiar velocity corrections remain a significant source of uncertainty. (An average peculiar velocity correction of 250 km s^{-1} is about 30% of the recession velocity of 679 km s^{-1} for NGC 4258.) For the total sample of six galaxies, Pesce et al. found values of H_0 ranging from 71.8 to 76.9 km s^{-1} Mpc^{-1}, depending on what assumptions are made and/or which models are adopted for the peculiar velocities.

In Figure 10, we show a comparison of several recent determinations of H_0 and their published uncertainties. Plotted are the relative PDFs, color-coded as labeled in the legend and including the TRGB (this paper), Cepheids (R21), those based on early-universe measurements (CMB; Planck Collaboration et al. 2020), the Dark Energy Survey Year 3 + BAO + BBN (DES Collaboration et al. 2021), gravitational-wave sirens (Hotokezaka et al. 2019), Miras (Huang et al. 2020), surface brightness fluctuations (SBF; Blakeslee et al. 2021; Khetan et al. 2021), masers (Reid et al. 2019), and recent results from strong lensing (Birrer et al. 2020). The Planck, DES Year 3 + BAO + BBN, TRGB, and Cepheid PDFs are also explicitly labeled.

From this figure, the discrepancy between the early universe (CMB + BAO) and local Cepheid measurements of H_0 is apparent, as is the difference between the TRGB and Cepheid

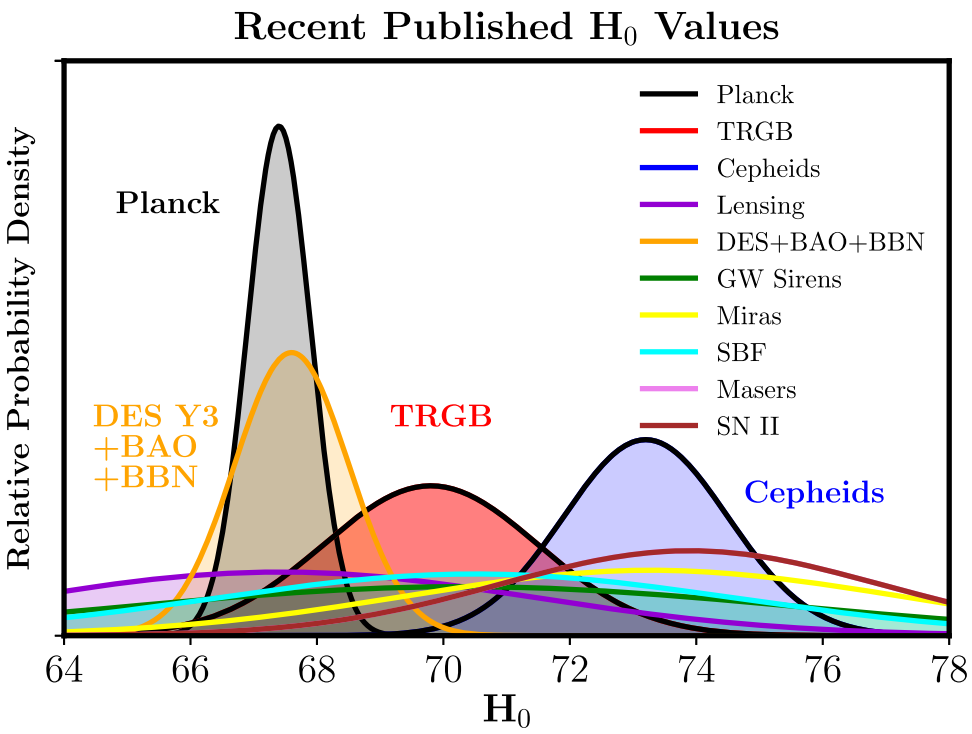

Figure 10. Relative PDFs for several current methods for measuring H_0. The CMB, BAO, strong lensing, and TRGB methods currently yield lower values of H_0, while Cepheids yield the highest values. The uncertainties associated with H_0 measurements from gravitational-wave sirens, strong lensing, Miras, masers, and SBF are currently significantly larger than the errors quoted for the TRGB and Cepheids. See text for details. (CMB: Planck Collaboration 2018; TRGB: this paper; Cepheids: R21; lensing: Birrer et al. 2020; DES Y3 + BAO + BBN: DES Collaboration et al. 2021; GW sirens: Hotokezaka et al. 2019; Miras: Huang et al. 2018; SBF: Khetan et al. 2021; masers: Reid et al. 2019).

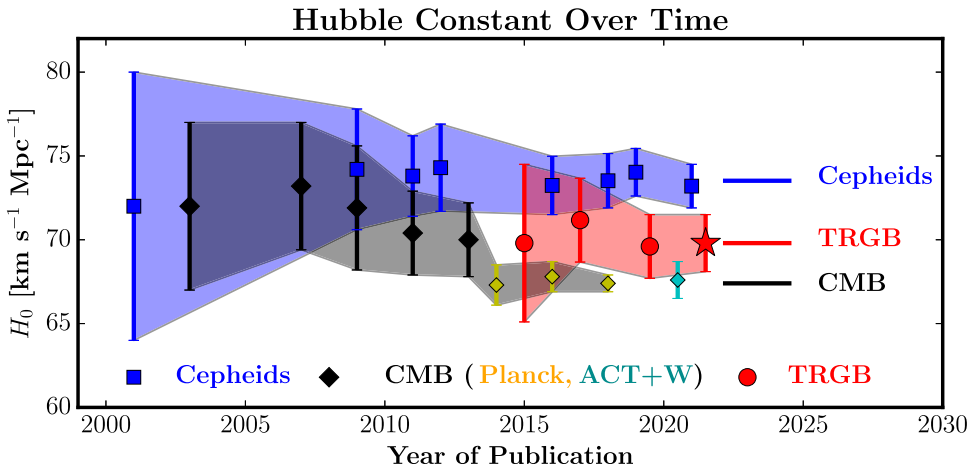

Figure 11. Summary of Hubble constant values in the past two decades based on Cepheid variables (blue squares), the TRGB (red circles and star), and estimates based on measurements of fluctuations in the CMB (WMAP: black diamonds; Planck: yellow diamonds; ACT + WMAP: cyan diamond). The CMB H_0 values assume a flat ΛCDM model. The CMB and Cepheid results straddle a range of 67–74 km s^{-1} Mpc^{-1}, with the TRGB results falling in the middle and overlapping the CMB results. The tension between the CMB and TRGB results amounts to only 1.3σ.

local determinations. Both the TRGB and Cepheid measurements have smaller uncertainties than the other (local) methods shown. These two methods currently have the largest samples of nearby objects (19 in both cases) that tie directly into the Hubble flow via SNe Ia. In Figure 11, the values of H_o as a function of time are shown for those based on measurements of the CMB, as well as those from the TRGB and Cepheid calibrations of SNe Ia.

Thus, the current situation is that there are two different types of tensions in play: (1) that between Cepheid measurements and the early universe and (2) that between Cepheid measurements and the TRGB.

For completeness, in the Appendix, we show a plot of 1065 H_0 values as a function of time for published data since 1980 (I. Steer 2021, private communication), as well as their histogram distribution. Interestingly, there is no bimodality (67 versus 73)

seen in the overall distribution of the recently published H_0 values, as can be seen in Figure A2.

8. Summary

In this paper, we have provided an update on the calibration of the absolute *I*-band magnitude of the TRGB anchored using several independent geometric zero-points. This updated calibration includes (1) extensive measurements of the TRGB over a wide area in the halo of the maser galaxy NGC 4258 (Jang et al. 2021), (2) independent observations of the TRGB in 46 Milky Way globular clusters covering a wide range of metallicities (Cerny et al. 2020), and (3) a reanalysis of the TRGB incorporating revised reddening corrections for the LMC and SMC (Hoyt 2021). These calibrations all agree with that earlier determined for the LMC alone (F19, F20) to better than 1%, providing multiple consistency checks on the LMC calibration of F19 and F20. Each of these calibrations is tied to geometrical distance anchors (H_2O megamasers in the case of NGC 4258, DEB distances and Gaia EDR3 parallaxes for the Milky Way globular clusters, and DEB distances for the LMC and SMC). In addition, using a fiducial horizontal branch sequence defined by the Milky Way globular clusters, we discuss and compare the TRGB absolute magnitude for the nearby dwarf elliptical galaxies Sculptor (Tran et al. 2021) and Fornax (Oakes et al. 2021) and four LMC globular clusters, finding excellent additional agreement.

An improved value of H_0 is determined by applying this new TRGB calibration to a sample of distant SNe Ia. This measurement is based on (1) the new calibration of the absolute *I*-band magnitude of the TRGB ($M_{\rm F814W}^{\rm TRGB} = -4.049 \pm 0.015\,({\rm stat}) \pm 0.035\,({\rm sys})$ mag) presented in this paper, (2) HST/ACS observations of TRGB stars in the halos of nearby galaxies known to host SNe Ia (F19, F20; Hoyt et al. 2021), and (3) a sample of 99 well-observed SNe Ia with multiwavelength photometry from the CSP (Krisciunas et al. 2017). Our final adopted value is

$$H_0 = 69.8 \pm 0.6\,({\rm stat}) \pm 1.6\,({\rm sys})\ {\rm km\ s^{-1}\ Mpc^{-1}}. \quad (6)$$

This value of H_0, based on the TRGB, agrees to within 1.3% with that inferred from modeling of the CMB observations.

Currently, the TRGB method and Cepheids provide the largest (statistically robust) and strongest (tested for systematics) base of distance determinations for the calibration of H_0 in the local universe. Together, they provide a check on the overall systematics. It is a testament to each method that a comparison for the nearest galaxies (i.e., within 7 Mpc) agrees in both zero-point and scatter to better than 2% accuracy (F19). However, these same two distance scales diverge at larger distances. It is important to understand the source of this divergence and ascertain whether its resolution will strengthen or weaken the case for additional physics. The fact that any given galaxy must have a unique distance means that systematic errors in one or both of the current estimates must be the cause for the divergence. At this time, the outcome is unknown; no clear evidence for outstanding systematic effects in either the TRGB or Cepheid distances has been found. It should be noted, however, that crowding/blending effects are not an issue for the TRGB, multiple geometric determinations of the zero-point show consistency at the 1% level, and metallicity effects are better understood from theory and more easily addressed empirically for TRGB stars than for Cepheids. Finally, a number of ongoing studies of the TRGB and Cepheids, the upcoming launch of JWST, and improvements to the Gaia zero-points in future releases all hold promise for significant improvement leading to a resolution of the current discrepancies within the next few years.

Support for program No. 13691 was provided by NASA through a grant from the Space Telescope Science Institute, which is operated by the Association of Universities for Research in Astronomy, Inc., under NASA contract NASA 5-26555. The CSP-I has been supported by the National Science Foundation under grants AST0306969, AST0607438, AST1008343, AST1613426, and AST1613472. Computing resources used for this work were made possible by a grant from the Ahmanson Foundation. This research has made use of the NASA/IPAC Extragalactic Database (NED), which is operated by the Jet Propulsion Laboratory, California Institute of Technology, under contract with the National Aeronautics and Space Administration. Some of the data presented in this paper were obtained from the Mikulski Archive for Space Telescopes (MAST). The STScI is operated by the Association of Universities for Research in Astronomy, Inc., under NASA contract NAS5-26555. I thank the Observatories of the Carnegie Institution for Science and the University of Chicago for their support of long-term research into the calibration and determination of the expansion rate of the universe. My thanks to many collaborators who have contributed to various facets of this research on the TRGB, Cepheids, and supernovae, in particular Barry Madore for his many decades of collaboration on the distance scale, as well as current and previous students Taylor Hoyt, William Cerny, Quang Tran, Elias Oakes, Kayla Owens, Finian Ashmead, and Dylan Hatt; postdoctoral fellows In Sung Jang, Rachael Beaton, and Jill Neeley; and research scientists and faculty Andy Monson, Mark Phillips, Mark Seibert, Jeff Rich, and Myung Gyoon Lee. Special thanks to Chris Burns for rerunning his SNooPy and STAN MCMC code on the CCHP TRGB sample updated since 2020 and for creating Figure 6. In addition, I gratefully acknowledge Ian Steer for providing access to his H_0 database. I thank Barry Madore, Kayla Owens, In Sung Jang, and Taylor Hoyt for their comments on the manuscript, as well as an anonymous referee for several helpful suggestions to update and improve the paper.

Facility: HST (ACS) Gaia.

Software: Matplotlib, NumPy, SciPy.

Appendix
Hubble Constants Published since 1980

Figure A1 plots H_0 values published since 1980. The scatter in published H_0 values has continued to decrease with time. All methods are included, without judgment as to the accuracy of a given method. In this sense, it is an unbiased sample.

Figure A2 shows in histogram form the distribution of H_0 values. It illustrates clearly how the scatter in H_0 values has decreased over the past four decades. For the most recent decade (2010–2020), the average, median, and mode of the H_0 distribution are 68.9, 68.6, and 68.0 ${\rm km\,s^{-1}\,Mpc^{-1}}$, respectively. The values of H_0 inferred from measurements of the CMB are shown in black. Interestingly, no obvious bimodality of H_0 values is seen between the values of 67 and 74 ${\rm km\,s^{-1}\,Mpc^{-1}}$, the two values that define the current "H_0 tension."

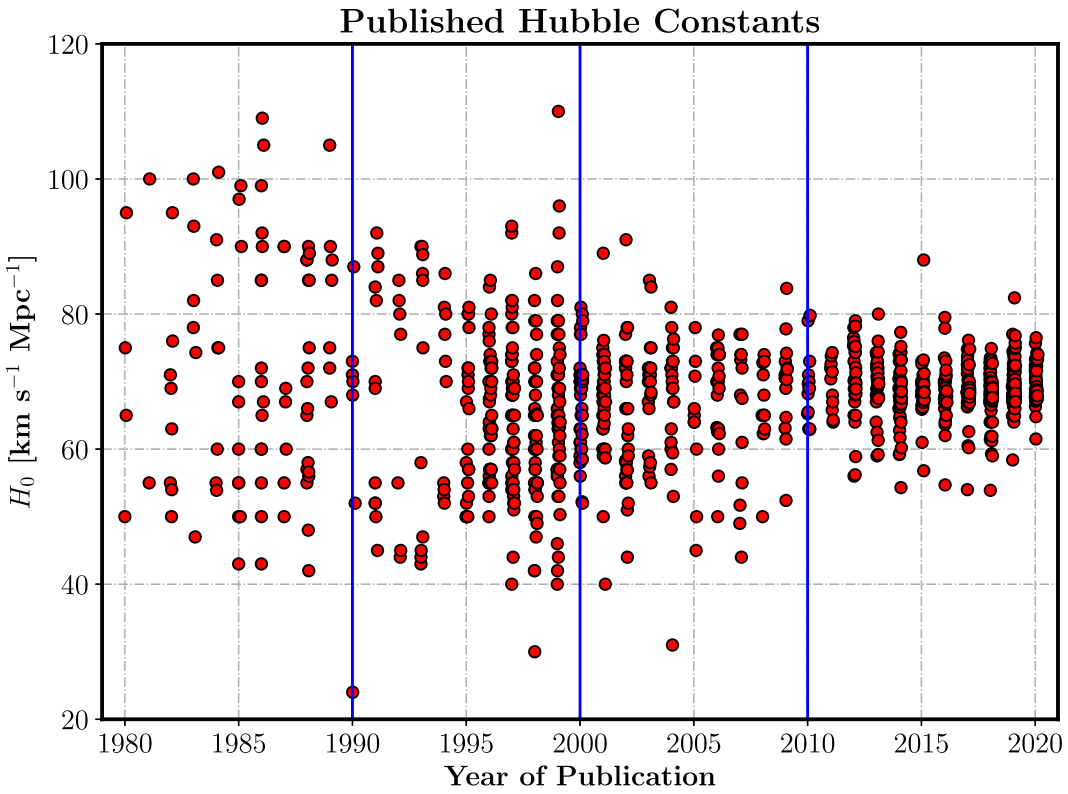

Figure A1. Plot of published H_0 values since 1980. The data are courtesy of I. Steer (2021, private communication). These data provide an update of the John Huchra Hubble constant database originally maintained for the NASA HST Key Project on the extragalactic distance scale (Freedman et al. 2001). This figure further updates that shown in Steer (2020) with an additional 99 entries.

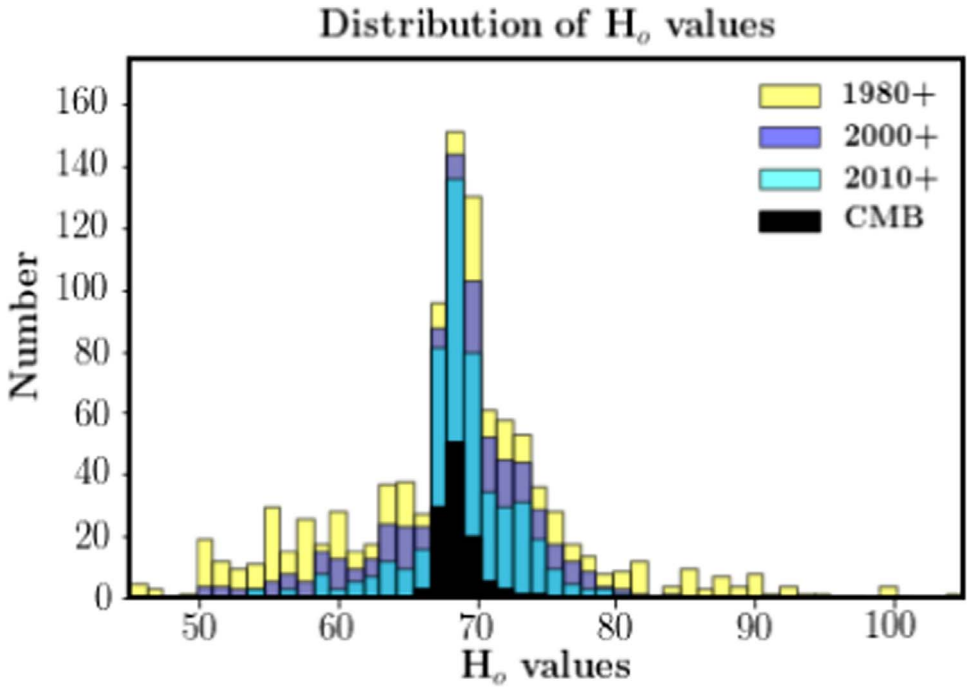

Figure A2. Histogram distributions of H_0 values for all published data since 1980 (yellow), 2000 (purple), and 2010 (cyan) and H_0 estimates from CMB data (black). The data source is the same as for Figure A1.

ORCID iDs

Wendy L. Freedman https://orcid.org/0000-0003-3431-9135

References

Aiola, S., Calabrese, E., Maurin, L., et al. 2020, JCAP, 2020, 047
Arenou, F., Luri, X., Babusiaux, C., et al. 2018, A&A, 616, A17
Aubourg, É., Bailey, S., Bautista, J. E., et al. 2015, PhRvD, 92, 123516
Bailer-Jones, C. A. L., Rybizki, J., Fouesneau, M., Demleitner, M., & Andrae, R. 2021, AJ, 161, 147
Baumgardt, H., & Vasiliev, E. 2021, MNRAS, 505, 5957
Bellazzini, M. 2008, MmSAI, 79, 440
Bellazzini, M., Ferraro, F. R., & Pancino, E. 2001, ApJ, 556, 635
Bellazzini, M., Ferraro, F. R., Sollima, A., Pancino, E., & Origlia, L. 2004, A&A, 424, 199
Benedict, G. F., McArthur, B. E., Feast, M. W., et al. 2007, AJ, 133, 1810
Birrer, S., Shajib, A. J., Galan, A., et al. 2020, A&A, 643, A165
Birrer, S., & Treu, T. 2021, A&A, 649, A61
Blakeslee, J. P., Jensen, J. B., Ma, C.-P., Milne, P. A., & Greene, J. E. 2021, ApJ, 911, 65
Bono, G., Caputo, F., Fiorentino, G., Marconi, M., & Musella, I. 2008a, ApJ, 684, 102
Bono, G., Stetson, P. B., Sanna, N., et al. 2008b, ApJL, 686, L87
Braga, V. F., Stetson, P. B., Bono, G., et al. 2018, AJ, 155, 137
Bressan, A., Marigo, P., Girardi, L., et al. 2012, MNRAS, 427, 127
Breuval, L., Kervella, P., Wielgórski, P., et al. 2021, ApJ, 913, 38
Burns, C. R., Ashall, C., Contreras, C., et al. 2020, ApJ, 895, 118
Burns, C. R., Parent, E., Phillips, M. M., et al. 2018, ApJ, 869, 56
Carpenter, B., Gelman, A., Hoffman, M., et al. 2017, J. Stat. Softw., 76, 1
Carretta, E., & Bragaglia, A. 1998, A&A, 329, 937
Cerny, W., Freedman, W. L., Madore, B. F., et al. 2020, arXiv:2012.09701
Da Costa, G. S., & Armandroff, T. E. 1990, AJ, 100, 162
Dalcanton, J. J., Williams, B. F., Melbourne, J. L., et al. 2012, ApJS, 198, 6
DES Collaboration, Abbott, T. M. C., Aguena, M., et al. 2021, arXiv:2105.13549
Di Valentino, E., Mena, O., Pan, S., et al. 2021, CQGra, 38, 143001
Durbin, M. J., Beaton, R. L., Dalcanton, J. J., Williams, B. F., & Boyer, M. L. 2020, ApJ, 898, 57
Efstathiou, G. 2020, arXiv:2007.10716
El-Badry, K., Rix, H.-W., & Heintz, T. M. 2021, MNRAS, 506, 2269
Fabricius, C., Luri, X., Arenou, F., et al. 2021, A&A, 649, A5
Fausnaugh, M. M., Kochanek, C. S., Gerke, J. R., et al. 2015, MNRAS, 450, 3597
Feeney, S. M., Mortlock, D. J., & Dalmasso, N. 2018, MNRAS, 476, 3861
Ferraro, F. R., Messineo, M., Fusi Pecci, F., et al. 1999, AJ, 118, 1738
Freedman, W. L., & Madore, B. F. 1990, ApJ, 365, 186
Freedman, W. L., Madore, B. F., Gibson, B. K., et al. 2001, ApJ, 553, 47
Freedman, W. L., Madore, B. F., Hatt, D., et al. 2019, ApJ, 882, 34
Freedman, W. L., Madore, B. F., Hoyt, T., et al. 2020, ApJ, 891, 57
Freedman, W. L., Madore, B. F., Hoyt, T., et al. 2021, JWST Proposal Cycle 1, 1995
Freedman, W. L., Madore, B. F., Rigby, J., Persson, S. E., & Sturch, L. 2008, ApJ, 679, 71
Freedman, W. L., Madore, B. F., Scowcroft, V., et al. 2011, AJ, 142, 192
Freedman, W. L., Madore, B. F., Scowcroft, V., et al. 2012, ApJ, 758, 24
Freedman, W. L., Wilson, C. D., & Madore, B. F. 1991, ApJ, 372, 455
Gaia Collaboration, Brown, A. G. A., Vallenari, A., et al. 2021, A&A, 649, A1
Gall, C., Stritzinger, M. D., Ashall, C., et al. 2018, A&A, 611, A58
Graczyk, D., Pietrzyński, G., Thompson, I. B., et al. 2020, ApJ, 904, 13
Harris, W. E. 1996, AJ, 112, 1487
Harris, W. E. 2010, arXiv:1012.3224
Hotokezaka, K., Nakar, E., Gottlieb, O., et al. 2019, NatAs, 3, 940
Hoyt, T. J. 2021, arXiv:2106.13337
Hoyt, T. J., Beaton, R. L., Freedman, W. L., et al. 2021, ApJ, 915, 34
Hoyt, T. J., Freedman, W. L., Madore, B. F., et al. 2018, ApJ, 858, 12
Huang, C. D., Riess, A. G., Hoffmann, S. L., et al. 2018, ApJ, 857, 67
Huang, C. D., Riess, A. G., Yuan, W., et al. 2020, ApJ, 889, 5
Humphreys, E. M. L., Reid, M. J., Moran, J. M., Greenhill, L. J., & Argon, A. L. 2013, ApJ, 775, 13
Jang, I. S., Hatt, D., Beaton, R. L., et al. 2018, ApJ, 852, 60
Jang, I. S., Hoyt, T. J., Beaton, R. L., et al. 2021, ApJ, 906, 125
Jang, I. S., & Lee, M. G. 2017, ApJ, 835, 28
Kennicutt, R. C. J., Stetson, P. B., Saha, A., et al. 1998, ApJ, 498, 181
Khetan, N., Izzo, L., Branchesi, M., et al. 2021, A&A, 647, A72
Kourkchi, E., Tully, R. B., Anand, G. S., et al. 2020, ApJ, 896, 3
Krisciunas, K., Contreras, C., Burns, C. R., et al. 2017, AJ, 154, 211
Lee, M. G., Freedman, W. L., & Madore, B. F. 1993, ApJ, 417, 553
Lee, Y.-W., Demarque, P., & Zinn, R. 1990, ApJ, 350, 155
Lindegren, L., Bastian, U., Biermann, M., et al. 2021a, A&A, 649, A4
Lindegren, L., Hernández, J., Bombrun, A., et al. 2018, A&A, 616, A2
Lindegren, L., Klioner, S. A., Hernández, J., et al. 2021b, A&A, 649, A2
Lindegren, L., Lammers, U., Bastian, U., et al. 2016, A&A, 595, A4
Linder, E. V. 2021, arXiv:2105.02903
Macaulay, E., Nichol, R. C., Bacon, D., et al. 2019, MNRAS, 486, 2184
Macri, L. M., Calzetti, D., Freedman, W. L., et al. 2001, ApJ, 549, 721
Macri, L. M., Stanek, K. Z., Bersier, D., Greenhill, L. J., & Reid, M. J. 2006, ApJ, 652, 1133
Madore, B. F. 1976, The Galaxy and the Local Group, Vol. 182 (Greenwich: Royal Greenwich Observatory), 153
Madore, B. F. 1982, ApJ, 253, 575
Madore, B. F., & Freedman, W. L. 1991, PASP, 103, 933
Madore, B. F., & Freedman, W. L. 2020, AJ, 160, 170
Madore, B. F., Freedman, W. L., Hatt, D., et al. 2018, ApJ, 858, 11
Madore, B. F., Mager, V., & Freedman, W. L. 2009, ApJ, 690, 389
Maíz Apellániz, J., Pantaleoni González, M., & Barbá, R. H. 2021, A&A, 649, A13
Marigo, P., Girardi, L., Bressan, A., et al. 2017, ApJ, 835, 77
McGonegal, R., McAlary, C. W., Madore, B. F., & McLaren, R. A. 1982, ApJL, 257, L33
Ménard, B., Scranton, R., Fukugita, M., & Richards, G. 2010, MNRAS, 405, 1025
Mignard, F., Klioner, S. A., Lindegren, L., et al. 2018, A&A, 616, A14
Monson, A. J., Freedman, W. L., Madore, B. F., et al. 2012, ApJ, 759, 146
Mortsell, E., Goobar, A., Johansson, J., & Dhawan, S. 2021, arXiv:2105.11461
Oakes, E., Hoyt, T., Freedman, W., et al. 2021, ApJ, in press
Olsen, K. A. G., Hodge, P. W., Mateo, M., et al. 1998, MNRAS, 300, 665
Owens, K., Freedman, W. L., Madore, B. F., et al. 2021, ApJ, in press
Pesce, D. W., Braatz, J. A., Reid, M. J., et al. 2020, ApJL, 891, L1
Pietrzyński, G. 2019, Natur, 567, 200
Planck Collaboration, Aghanim, N., Akrami, Y., et al. 2020, A&A, 641, A6
Prusti, T., Gaia Collaboration, de Bruijne, J. H. J., et al. 2016, A&A, 595, A1
Reid, M. J., Pesce, D. W., & Riess, A. G. 2019, ApJL, 886, L27
Riess, A. G., Casertano, S., Yuan, W., et al. 2018, ApJ, 861, 126
Riess, A. G., Casertano, S., Yuan, W., et al. 2021, ApJL, 908, L6
Riess, A. G., Casertano, S., Yuan, W., Macri, L. M., & Scolnic, D. 2019, ApJ, 876, 85
Riess, A. G., Macri, L. M., Hoffmann, S. L., et al. 2016, ApJ, 826, 56
Riess, A. G., Yuan, W., Casertano, S., Macri, L. M., & Scolnic, D. 2020, ApJL, 896, L43
Ripepi, V., Catanzaro, G., Molinaro, R., et al. 2020, A&A, 642, A230
Rizzi, L., Tully, R. B., Makarov, D., et al. 2007, ApJ, 661, 815
Romaniello, M., Primas, F., Mottini, M., et al. 2008, A&A, 488, 731
Salaris, M., Cassisi, S., & Weiss, A. 2002, PASP, 114, 375
Schlafly, E. F., & Finkbeiner, D. P. 2011, ApJ, 737, 103
Scolnic, D. M., Jones, D. O., Rest, A., et al. 2018, ApJ, 859, 101
Scowcroft, V., Freedman, W. L., Madore, B. F., et al. 2011, ApJ, 743, 76
Skowron, D. M., Skowron, J., Udalski, A., et al. 2021, ApJS, 252, 23
Soltis, J., Casertano, S., & Riess, A. G. 2021, ApJL, 908, L5
Steer, I. 2020, AJ, 160, 199
Stetson, P. B. 1987, PASP, 99, 191
Stetson, P. B. 1994, PASP, 106, 250
Stetson, P. B., Pancino, E., Zocchi, A., Sanna, N., & Monelli, M. 2019, MNRAS, 485, 3042
Suyu, S. H., Bonvin, V., Courbin, F., et al. 2017, MNRAS, 468, 2590
Tammann, G. A., Sandage, A., & Reindl, B. 2008, ApJ, 679, 52
Thompson, I. B., Kaluzny, J., Pych, W., et al. 2001, AJ, 121, 3089
Tran, Q., Hoyt, T., Freedman, W., et al. 2021, ApJ, in press
Tripp, R. 1998, A&A, 331, 815
Uddin, S. A., Burns, C. R., Phillips, M. M., et al. 2020, ApJ, 901, 143
Ulaczyk, K., Szymański, M. K., Udalski, A., et al. 2012, AcA, 62, 247
Vasiliev, E., & Baumgardt, H. 2021, MNRAS, 505, 5978
Verde, L., Treu, T., & Riess, A. G. 2019, NatAs, 3, 891
Wong, K. C., Suyu, S. H., Chen, G. C. F., et al. 2020, MNRAS, 498, 1420
Yuan, W., Riess, A. G., Macri, L. M., Casertano, S., & Scolnic, D. M. 2019, ApJ, 886, 61